DEMOCRATIC REPUBLIC OF ALGERIA
وزارة التعليم العالي و البحث العلمي
MINISTRY OF HIGHER EDUCATION AND SCIENTIFIC RESEARCH
جامعة عمار ثليجي بالأغواط
AMAR TELIDJI UNIVERSITY, LAGHOUAT
كلية التكنولوجيا
TECHNOLOGY FACULTY
قسم الكترونيك
ELECTRONIC DEPARTEMENT

Dissertation Master Degree in Microelectronic

Domain : Technology Sciences
Filiere : Electronics
Option : Microelectronic

Presented by

Guenou Nesrine

Theme

PERFORMANCE ENHANCEMENT OF PEROVSKITE SOLAR CELL FASnI3/FAGeCI$_3$

Sunday, 30th June 2024

Publicly supported in front of the jury composed of :

Dr. BIRANE Mouhoub	*MCA University of Laghouat*	President
Dr. BELLAKHDAR Aissa	*MCA University of Laghouat*	*Examiner*
Mme. VILBOIS Leila.Amal	*MAA University of Laghouat*	Supervisor

DEMOCRATIC REPUBLIC OF ALGERIA
وزارة التعليم العالي و البحث العلمي
MINISTRY OF HIGHER EDUCATION AND SCIENTIFIC RESEARCH
جامعة عمار ثليجي بالأغواط
AMAR TELIDJI UNIVERSITY, LAGHOUAT
كلية التكنولوجيا
TECHNOLOGY FACULTY
قسم الكترونيك
ELECTRONIC DEPARTEMENT

Dissertation Master Degree in Microelectronic

Domain : Technology Sciences
Filiere : Electronics
Option : Instrumentation

Presented by

Zaidi Nour Elhouda

Theme

PERFORMANCE ENHANCEMENT OF PEROVSKITE SOLAR CELL $FASnI_3/FAGeCI_3$

Sunday, 30th June 2024

Publicly supported in front of the jury composed of :

Dr. BIRANE Mouhoub	*MCA University of Laghouat*	President
Dr. BELLAKHDAR Aissa	*MCA University of Laghouat*	*Examiner*
Mme. VILBOIS Leila.Amal	*MAA University of Laghouat*	Supervisor

ACKNOWLEDGMENTS

First and foremost, we are very grateful to ALLAH S.W.T for giving us the key and opportunity to accomplish our master's dissertation.

We would like to express our sincere gratitude to our supervisor, Mme. Vilbois Leila, for her invaluable guidance, support, and constructive feedback throughout our master's program. Her expertise and encouragement were instrumental in completing this research and writing this dissertation.

We also appreciate the members of the jury for their time, expertise, and valuable feedback on our work.

Finally, we would like to thank all the professors, staff, and technicians in the Department of Electrical Engineering at Amar Telidji University of Laghouat for their cooperation and support.

DEDICATION

This work is dedicated first and foremost to my parents, whose unwavering love and faith that have been my greatest source of strength and inspiration.

Big thanks to my siblings for their constant support and for always standing by my side, and to my partner in this work Zaidi Nour elhouda who was more than just a collaborator.

I extend my deepest gratitude to Mme. Vilbois Leila for her invaluable guidance and support throughout the dissertation process.

Finally, a special thanks to Redwane who helped me along the way**.** Your unwavering support and shared knowledge fueled my journey and made this achievement possible.

Nesrine Guenou

Sincerely,

This thesis wouldn’t exist without the unwavering support of my family. Their constant encouragement and belief in me, not just my abilities, but in who I am as a person, fueled my journey. To myself, I offer deep gratitude for the perseverance, dedication, and hard work that brought this work to life.

My fiancé and friends deserve immense thanks for providing the encouragement and companionship that kept me going during challenging times. Your unwavering positivity was a source of immense comfort and joy. Special thanks to my thesis partner, Guenou Nesrine. Our collaboration was essential in overcoming obstacles and reaching milestones. Your dedication and teamwork made this journey not just productive, but truly enriching and rewarding.

To my supervisor, I express my sincere appreciation for your guidance and insightful advice throughout this research. Your commitment to my academic growth has been invaluable. Finally, to everyone who believes in the power of knowledge and the pursuit of excellence, your passion and dedication inspire me to keep striving for greatness and never stop learning. Thank you all for being my inspiration and unwavering support system.

Zaidi Nour Elhouoda

TABLE OF CONTENT

CHAPTER III SIMULATION OF THE FASNI3 SOLAR CELL

LIST OF FIGURES

Chapter I

Chapter II

Chapter III

LIST OF TABLES

LIST OF ABBREVIATIONS

ABX_3 - A, B, X-notation for perovskite crystal structure.

AC - Alternating Current (A).

AM - Air Mass.

ASCII - American Standard Code for Information InterchangeAngstrom.

CB - Conduction Band (eV).

CET - Coal Equivalent Ton (tce).

CVD - Chemical Vapor Deposition.

C – Capacitance (F).

C-f - Capacitance-Frequency (F/Hz).

C-V - Capacitance-Voltage (F/V).

CPV - Concentration Photovoltaics.

CV - Current-Voltage (A vs V).

DOS - Density of States ($eV^{-1}.cm^{-3}$).

EFG - Edge-defined Film-fed Growth.

ETL - Electron Transport Layer.

Eg - Forbidden Gap (eV).

ESCA - Electron Spectroscopy for Chemical Analysis.

eV - Electron Volt.

HOMO - Highest Occupied Molecular Orbital (eV).

HEED - High-Energy Electron Diffraction (eV).

HTL - Hole Transport Layer.

IR – Infrared (Hz) or (cm^{-1}).

J-V - Current-Voltage (A vs V).

LEED - Low-Energy Electron Diffraction.

LUMO - Lowest Unoccupied Molecular Orbital (eV).

MBE - Molecular Beam Epitaxy.

LIST OF ABBREVIATIONS

Na - Acceptor Concentration (cm^{-3}).

Nd - Donor Concentration (cm^{-3}).

Nt – Trap Density (cm^{-3}).

PB – Photobiological.

PC – Photochemical.

PCS - Perovskite Solar Cells.

PCE - Power Conversion Efficiency (%).

PV – Photovoltaic.

P_in - Incident power (W).

QE - Quantum Efficiency.

Rs - Series Resistance (Ω).

Rsh - Shunt Resistance (Ω).

SIMS - Secondary Ion Mass Spectrometer.

SUS/kWhr - United States Dollars per kilowatt-hour (USD/kWh).

UV – Ultraviolet (Hz) or (nm).

UHV - Ultra-High Vacuum (Pa).

VB - Valence Band (eV).

η – Efficiency (%).

μe - Electron Mobility (cm^2/Vs).

μh - Hole Mobility (cm^2/Vs).

ħ - Reduced Planck's Constant (J·s).

GENERAL INTRODUCTION

Solar cells are fundamental components of solar panels and are widely used in various applications, from powering small gadgets to providing electricity for homes and businesses.

One promising avenue in solar cell research is the use of perovskite materials. The perovskite solar cells (PSCs) represent a cutting-edge technology in the field of renewable energy, known for their remarkable efficiency and potential for low-cost production. PSCs have gained significant attention in recent years because they offer several advantages over traditional silicon-based solar cells, including easier fabrication processes, flexibility, and the ability to be produced with a variety of substrates. Despite challenges such as stability and scalability that still need to be addressed, perovskite solar cells hold promise for contributing significantly to the global transition towards sustainable energy.

In the first chapter we introduced the fundamental concepts of solar energy and semiconductor technology which are crucial for understanding solar cells, we also mentioned the different generations of solar cells that have been developed, as well as the elaboration methods and the equivalent circuit of a solar cell, detailing its components.

Chapter two focuses on perovskite solar cells, examining their significant advantages such as high efficiency and low production costs, as well as their disadvantages. The chapter highlights ($FASnI_3$), a specific type of perovskite material known for its eco-friendly properties and potential in solar applications. It delves into the properties of ($FASnI_3$), discussing its benefits and challenges, additionally recombination and charge transfer mechanisns.

Chapter Three presented a simulation on SCAPS applying to design and simulate a new lead-free perovskite solar device employing $FASnI_3$ as an absorber material. Starting with simulate our structure with and without the n^+-$FASnI_3$ layer, all this is to observe the effect of this layer and whether it increases efficiency.

CHAPTER I

THE BASICS OF PHOTOVOLTAIC ENERGY

I.1 INTRODUCTION

Solar cell technology has undergone significant evolution, representing a pivotalaspect of energy transition by enabling the direct conversion of sunlight into electricity using electronic materials. Initially developed for powering space missions, solar cells have now become essential components of terrestrial energy systems. Despite technological advancements, barriers persist in the photovoltaic system, prompting the search for alternatives to enhance compatibility and performance. This necessitates the development of cost-effective techniques and high-capacity cells through innovative materials, concepts, and thin films that minimize material using. Semiconductor material designs and precise control over electro-optical properties are crucial for optimal cell performance.

I.2 SOLAR ENERGY

I.2.1 Sun

The sun is the largest object in our solar system and one of the larger stars in our galaxy. It will continue to do so until the end of the earth's remaining life, which is predicted to be about 5×109 years. The diameter of the sun is R = 1.39 ×106 km. It is estimated that 90% of the energy isgenerated in the region between 0 and 0.23R, which contains 40% of the sun's mass. Thecore temperature varies between 8 ×106 K and 40 ×106 K and the density is estimated atabout 100 times that of water.

The sun radiates electromagnetic energy in terms of photons which are light particles. Almost one third of this incident energy on the earth is reflected back, but the rest is absorbedand is, eventually, retransmitted to deep space in terms of long-wave infrared radiation.Today, the earth radiates just as much energy as it receives and sits in a stable energy balanceat a temperature suitable for life on the earth. In fact, solar radiation is in the form of whitelight and it spreads over a wider spectrum of wavelengths from the short-wave infrared toultraviolet. The wavelength distribution is directly dependent on the temperature of the sun'ssurface. On the other hand, about 80% of the world's population lives between latitudes 35° N and 35° S. These regions receive the sun's radiation for almost 3000– 4000 h/year. In solar power density terms, this is equivalent to around 2000 kWh/year, which is 0.25 CET/year [1].

I.2.2 Photons and light

Electromagnetic radiation can be seen as a combination of electromagnetic waves or as packets of energy without mass, known as photons. This radiation can be categorized based on either its wavelength (λ) or frequency (ν), which are related by the equation:

$$\lambda = c_\gamma / \upsilon \quad \textbf{(I.1)}$$

The speed of light, denoted by cγ, depends on the refractive index (n_r) of the medium it travels through, given by the equation:

$$C_\gamma = c/n_r \quad \textbf{(I.2)}$$

The angular frequency is represented by $\omega = 2\pi\nu$, where h is Planck's constant and $\hbar = h/2\pi$. Photon energy can be converted into wavelength using the formula:

$$\lambda(nm) = 1240/h\nu\ (eV) \quad \textbf{(I.3)}$$

The electromagnetic spectrum consists of various parts, as depicted in **Figure I.1**. The optical region, crucial for solar energy conversion and lighting, encompasses the ultraviolet (UV) region, visible-light region (approximately λ = 0.4–0.7 μm), and the infrared (IR) region extending beyond the visible spectrum to about λ = 1000 μm. "Light" refers to the segment of the electromagnetic spectrum that elicits a visual response in humans.

The solar spectrum demonstrates two distinct patterns: the number of photons reaching the Earth's atmosphere and surface per wavelength interval. Approximately half of solar irradiation occurs beyond the visible range, particularly in the IR, providing radiant energy and heat rather than visible light. Spectral variations above and below the atmosphere stem from the selective filtering of specific wavelengths [2].

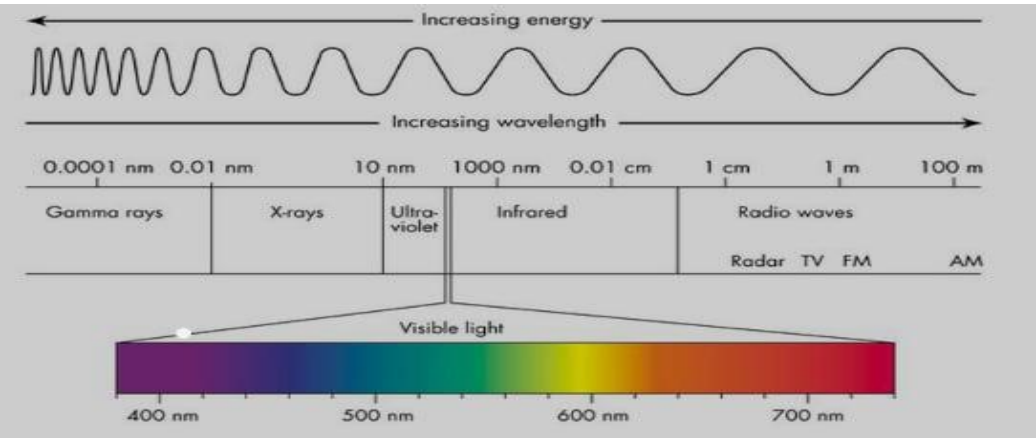

Fig I.1:*Electromagnetic spectrum in the range between microwaves and gamma rays [2].*

I.3 THE EXTRATERRESTRIAL RADIATION

Solar radiation originates from the Sun and closely resembles that emitted by a theoretical object known as a black body, with a temperature of approximately 5900°C.

When measured above the Earth's atmosphere, solar radiation exhibits an intensity of about 1.35 kilowatts per square meter (kW/m^2), with its spectral distribution predominantly centered around a wavelength of λ=0.48 μm.

However, upon reaching the Earth's surface, the power density of solar radiation diminishes to around 0.9 kW/m^2. This reduction is primarily attributed to the absorption of solar energy by various atmospheric constituents, including ozone, water vapor, and carbon dioxide.

Furthermore, as solar radiation traverses the atmosphere, its spectral composition undergoes alterations, manifesting as absorption bands rather than a continuous spectrum.

To accurately account for the effects of atmospheric attenuation on solar radiation, the concept of air mass (AM) is utilized. Air mass is mathematically defined as $AM=1/\cos(\alpha)$, where α represents the angle between the direction of the Sun's rays and the vertical axis.

Specifically, AM1.5 denotes solar radiation incident on the Earth's surface under clear sky conditions, with a surface area of one square meter inclined at an angle of 48° with respect to the equatorial plane.

It's essential to differentiate between AM1.5D and AM1.5G spectra, representing direct and global solar fluxes, respectively. AM1.5G encompasses both direct and diffuse solar radiation components.

Different air mass values correspond to specific positions of the Sun relative to the observer. For example, AM1 corresponds to the Sun being directly overhead (α=0), while AM4 indicates the Sun nearing the horizon (α=75°). Conversely, AM0 signifies conditions unaffected by atmospheric absorption, observed above the Earth's atmosphere [3].

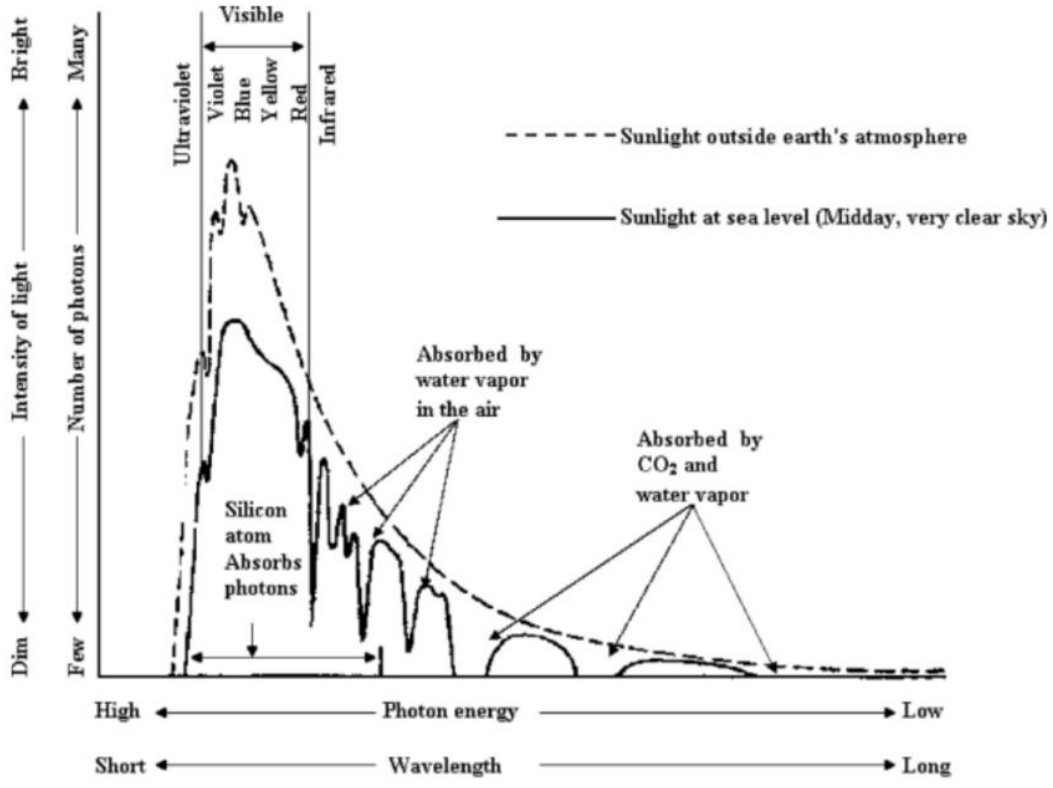

Fig I. 2: *Solar radiation spectrum [1].*

I.4 SEMICONDUCTOR

Semiconductor materials are of paramount importance in modern electronics, as they exhibit electrical conductivity values including between those of conductors, such as copper, and insulators, like glass. Their resistivity typically decreases as temperature rises, unlike metals. In many cases, their conductive properties can be intentionally altered by introducing impurities ("doping") into their crystal structure. The existence of two differently doped regions within the same crystal creates a semiconductor junction. The behavior of charge carriers electrons, ions, and holes at these junctions forms the basis of diodes, transistors, and various electronic devices.Semiconductor materials play a crucial role in modern electronics, enabling a wide range of functionalities, such as asymmetric conduction, variable resistance, and sensitivity to light or heat. This is achieved through the ability to modify their electrical properties via doping and the application of electric fields or light. Our modern understanding of semiconductor material properties relies heavily on quantum physics to explain the movement of charge carriers within the crystal lattice [4].

I.4.1 Intrinsic semiconductors

Intrinsic semiconductors, such as pure silicon, play a crucial role in modern electronics by serving as the foundation for various semiconductor devices. Understanding their behavior is essential for designing and optimizing electronic circuits.

A silicon crystal behaves differently from an insulator due to the presence of a finite probability that electrons can move freely within it, creating what is known as a hole. Both electrons and holes contribute to current flow when a voltage is applied. According to the band model of semiconductors, at normal temperatures, electrons transition to the conduction band, facilitating electrical conduction [5].

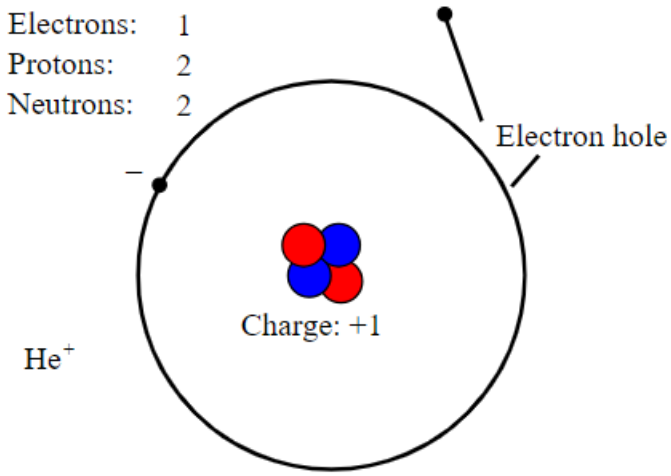

Fig I.3:*Electrons and holes [5]*.

The term "intrinsic" distinguishes pure silicon from doped "extrinsic" semiconductors, which are either N-type or P-type. In an intrinsic semiconductor, both electrons and holes contribute to current flow. This flow includes the movement of electrons and the displacement of holes throughout the material. Additionally, electrons can migrate between lattice positions to fill vacancies.

At temperatures above zero, intrinsic semiconductors like silicon exhibit electron excitation into the conduction band, leaving behind holes in the valence band. The introduction of dopants enhances conductivity by introducing additional electrons for N-type semiconductors and holes for P-type semiconductors. This process aids in balancing the charge carriers and improving conductivity.

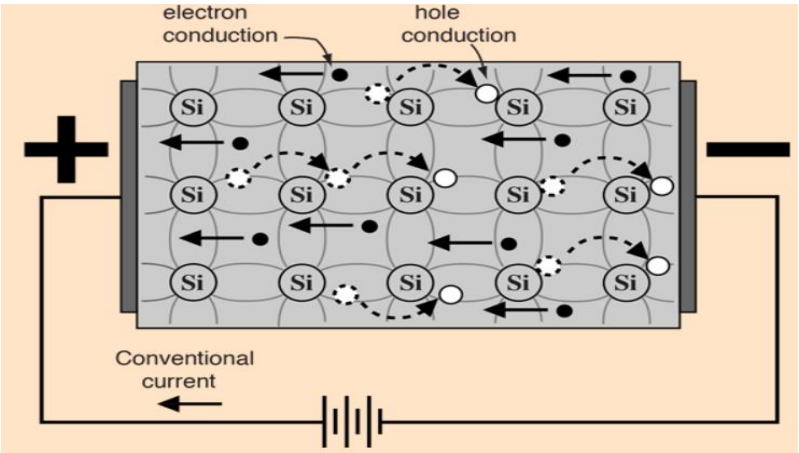

Fig I.4*: Semiconductor Current [5]*.

I.4.2 Extrinsic semiconductors

Extrinsic semiconductors are semiconductors that are doped with specific impurities. The impurity modifies the electrical properties of the semiconductor and makes it more suitable for electronic devices such as diodes and transistors.

While adding impurities, a small amount of suitable impurity is added to pure material, increasing its conductivity by many times. Extrinsic semiconductors are also called impurity semiconductors or doped semiconductors. The process of adding impurities deliberately is termed as doping and the atoms that are used as an impurity are termed as dopants. The impurity modifies the electrical properties of the semiconductor and makes it more suitable for electronic devices such as diodes and transistors.

The dopant added to the material is chosen such that the original lattice of the pure semiconductor is not distorted. Also, the dopants occupy only a few of the sites in the crystal of the original semiconductor, and it is necessary that the size of the dopant is nearly equal to the size of the semiconductor atoms [5].

I.4.3 Some Commonly Used Dopants

While doping tetravalent atoms such as Si or Ge, two types of dopants are used, and they are:

- **Pentavalent atoms**: Atoms with valency 5; such as Arsenic (As), Phosphorous (Pi), Antimony (Sb), etc.
- **Trivalent atoms**: Atoms with valency 3; such as Indium (In), Aluminium (Al), Boron (B), etc.

The reason behind using these dopants is to have similar-sized atoms as the pure semiconductor. Both Silicon and Germanium atoms belong to the fourth group in the periodic table. Hence, the choice of dopants from the third and fifth group is more viable. This ensures that the size of the atoms is not very different from the fourth group. Therefore, the trivalent and pentavalent choices. These dopants give rise to two types of semiconductors as follows:

- **n-type semiconductors**
- **p-type semiconductor**

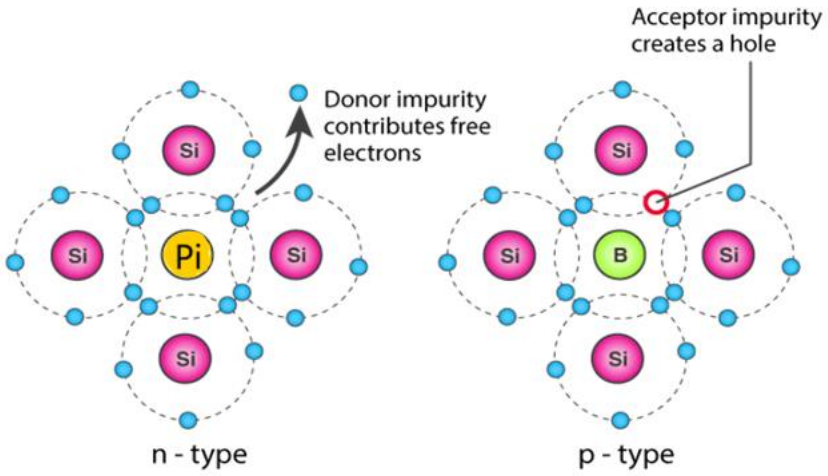

Fig I.5*: Extrinsic Semiconductors.*

To keep P-Type semiconductors one needs to dope silicon with trivalent impurities such as:

Boron, Aluminum and Gallium. These create lack of valence electrons.

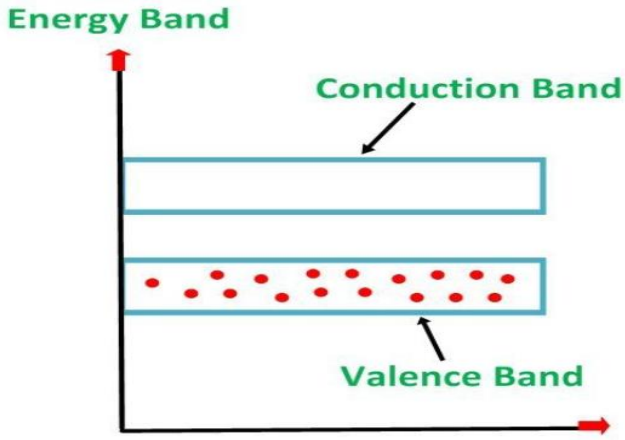

Fig I.6*: Energy bands of t-type semiconductor [5]*.

I.4.4 The PN junction

the junction is formatted by the juxtaposition of different types in a semi-conductor monocrystalline. These different regions affect the skin and nature of its impurities.

It ispossible to use different types of semi-conductors, such as “heterojunctions” [6].

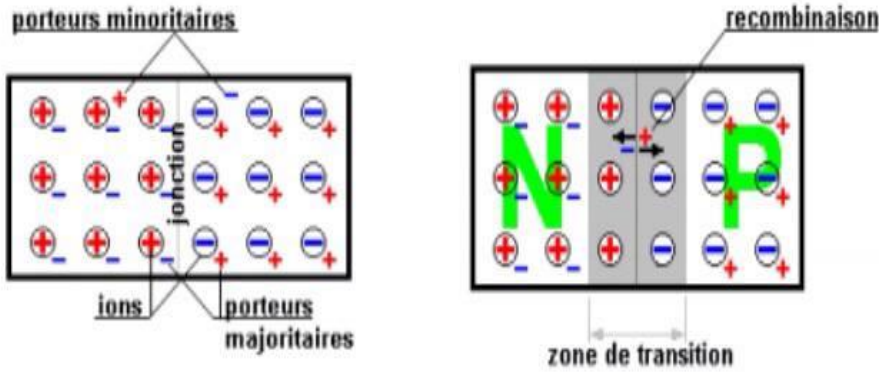

Fig I.7*: Formation of a PN junction.*

I.3.4. Energy bands:

At a PN junction in thermodynamic equilibrium, the Fermi level on both the P-doped and N-doped sides aligns. This alignment causes a curvature in the conduction and valence bands near the junction in the energy diagram.

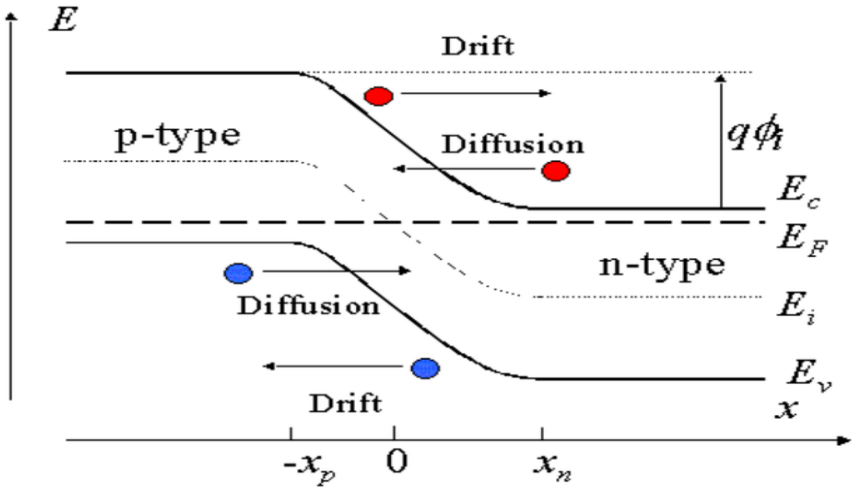

Fig I.8*: Energy band diagram of PN Junction under Equilibrium* [7].

I.5 SOLAR CELLS

Solar cells are semi-conductor devices which use sunlight to produce electricity. They are manufactured and processed in a similar fashion as computer memory chips.

Solar cells are primarily made up of silicon which absorbs the photons emitted by sun's rays. The process was discovered as early as 1839. Silicon wafers are doped and the electrical contacts are put in place to connect each solar cell to another. The resulting silicon disks are given an anti-reflective coating. This coating protects sunlight loss. The solar cells are then encapsulated and placed in an aluminium frame. The process requires continuous monitoring to ensure quality control over a period of time. After the manufacturing process is complete, they undergo final test to check their efficiency under normal conditions [8].

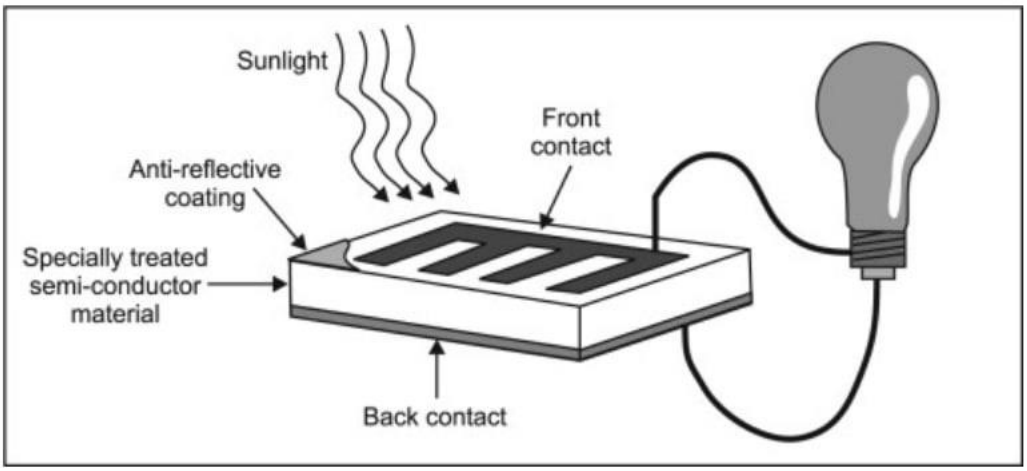

Fig I.9*: Solar cells.*

I.5.1 Solar cell structure

A solar cell consists of a layer of p-type silicon placed next to a layer of n-type silicon (**Figure I.10**). In the n-type layer, there is an excess of electrons, and in the p-type layer, there is an excess of positively charged holes (which are vacancies due to the lack of valence electrons). Near the junction of the two layers, the electrons on one side of the junction (n-type layer) move into the holes on the other side of the junction (p-type layer). This creates an area around the junction, called the depletion zone, in which the electrons fill the holes [9].

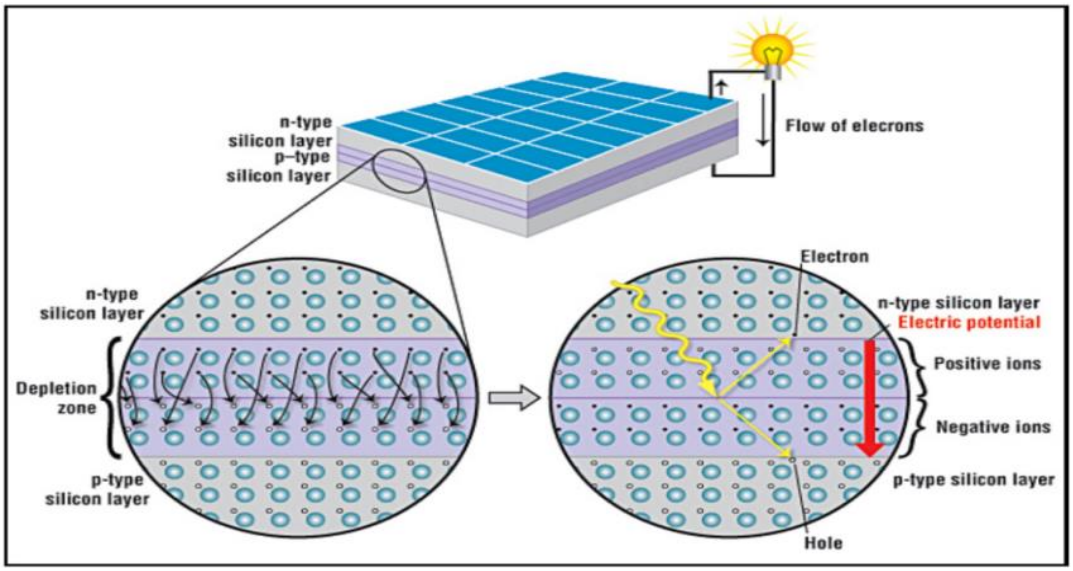

Fig I.10*: Schematic representation of a solar cell, showing the n-type and p-type layers, with a close-up view of the depletion zone around the junction between the n-type and p-type layers.*

I.5.2 Types of solar cells

I.5.2.1 First Generation Solar Cells

I.5.2.1.1 Crystalline Silicon

I.5.2.1.1.1 Monocrystalline silicon cells:

Monocrystalline panels are made of single-crystal silicon, which is melted into bars, cut into wafers, and treated with anti-reflective coating that improves its efficiency and gives it a darker appearance.

Although these aesthetically pleasing black solar panels are more expensive than other options, they're also the most efficient panel for domestic households [10].

I.5.2.1.1.2 Polycrystalline silicon cells:

Polycrystalline solar panels are made by melting multiple silicon crystals and pouring them into a square mould, which creates this panel's blue mosaic look.

They're slightly more eco-friendly than their monocrystalline counterparts, because less silicon is wasted during the process, and they're often the cheaper option.

However, polycrystalline panels cost more per watt of power output, because they're about one-third less efficient than monocrystalline panels [10].

I.5.2.2 Second Generation Solar Cells

I.5.2.2.1 Thin film solar cell technology:

Thin film solar panels are created by placing several thin layers of photovoltaic material – amorphous silicon, cadmium telluride, copper indium gallium selenide, or organic PV cells – on top of each other.

Depending on the material, their efficiency rating ranges from 7% to 13%.

This means **thin film panels have a much lower efficiency rating than other types of solar panels,** but their main asset is their flexibility [10].

Amorphous Silicon solar cells, Copper Indium Gallium Di-Selenide [CIGS], Thin-Film Cadmium Telluride Solar Cell Technology, Copper Zinc Tin Sulphide Thin film solar cells, Compounds of group III-V.

I.5.2.3 Third Generation Solar Cells:

The latest solar cell technologies combine the best features of crystalline silicon and thin-film solar cells to provide high efficiency and improved practicality for use. They tend to made from amorphous silicon, organic polymers or perovskite crystals, and feature multiple junctions made up from layers of different semiconducting materials.

I.5.2.3.1 Perovskite solar cells:

Perovskite solar panels are made using perovskite, a synthetic material inspired by the crystal structure of a mineral with the same name.

This material is layered on top of standard silicon to form a tandem model. Silicon can already absorb the red end of the solar spectrum, but perovskite is able to absorb the blue part.

It's able to reach efficiencies like 33.7%, which a team of scientists in Saudi Arabia achieved in May 2023 with a single perovskite-silicon cell.

In the same month, British company Oxford PV announced that its full-sized panel has attained 28.6% efficiency [10].

I.5.2.3.2 Organic Solar Cell:

Photovoltaic technology that uses organic semiconductor electronics is organic solar cell technology which deals with conductive organic polymers or small organic molecules such that light is absorbed and charge carriers are produced by Photovoltaic effect [11]. Most organic photovoltaic cells are polymer solar cells composed of conjugated polymers or small organic semiconductor molecules. Some characteristics of Organic solar cells are (a) It combines the virtues of plastics with those of semiconductors (b) High optical absorption coefficients (c) Properties tuned with flexible synthesis (d) Lowcost fabrication. Either Bilayer or Bulk hetero-junction architecture can be used for organic solar cell fabrication [12].

I.5.2.3.3 Hetrojunction Technology:

The silicon heterojunction solar cell is based on a device structure that combines thin film and bulk silicon technology of particular interest is the heterojunction cell with an intrinsic thin layer (HIT) with which Sanyo had achieved a very high efficiency of 23% in 2009, and of 25.6% efficiency most recently. This strongly challenges the standard high efficiency c-Si homojunction cell [13].

I.5.2.4 Future of Solar cell Technology:

Solar cell technology is vast field in which, we can harness a large amount of solar energy incident on Earth's surface. Large solar panels are required to capture incident sunlight. This transformed energy can be stored and used in different applications. Erecting large solar panels and maintaining these solar panels could become cumbersome and hectic. Moreover, large landscape is wasted for erecting these solar panels. In Asian countries land available per square feet for an individual is very less and erection of large Solar panels would cause crisis of land. More advanced and smart solar panels can be designed to overcome this problem [12].

Table I.1: Cost, Efficiency, Durability of each type [13] .

Type of solar panel	Cost per m^2	Efficiency (%)	Lifespan (years)
Monocrystalline	59200 Da	18-24	25-40
Polycrystalline	47360 Da	13-16	25-30
Thin film	16745 Da	7-13	10-20
Perovskite		28.6-33.7	25-30

I.5.3 Elaboration methods and technics

I.5.3.1 Method of epitaxy

Epitaxy refers to the process of depositing a thin overlayer on a crystalline substrate, where the overlayer aligns structurally with the substrate.

I.5.3.2 Hot wall epitaxy

Hot wall epitaxy involves using one or two annular vapor sources, with vapors transported through a heated cylindrical enclosure maintained at a higher temperature than the substrate. This process results in the deposition of homogenized and equilibrated multicomponent vapors on the substrate. This technique has been successfully employed to produce high-quality epitaxial films of various IV-VI and II-VI compounds.

I.5.3.3 Molecular beam epitaxy

Molecular Beam Epitaxy (MBE) is a technique for growing epitaxial layers on a single crystal substrate using directed beams of atoms or molecules in an ultrahigh-vacuum (UHV) system. This method allows precise control of deposition rates, enabling high-quality growth at lower temperatures and the formation of complex multilayer structures. MBE is particularly useful for creating quantum-well superstructures, heterostructures, and specialized microelectronic applications. It is widely used for depositing II-VI and III-V compounds, including GaAs-based heterojunctions.

I.5.3.4 Graphoepitaxy

Graphoepitaxy is a technique where vapor-deposited films on patterned amorphous substrates achieve orientation. Smith and colleagues showed that silicon films deposited on a grating-patterned SiO_2 substrate can be fully oriented by laser crystallization. The grating's spacing must be smaller than the film's grain size. This method holds potential for creating large-area crystalline films, useful in applications such as solar cells.

I.5.3.5 Sputtering technique

When a material is bombarded by energetic entities such as accelerated ions, atoms are ejected from its surface, a phenomenon known as back sputtering. The simplest practical sputtering reactor is a diode sputtering system, consisting of an anode and a cathode in a vacuum chamber filled with gas, typically argon. The target material, part of the cathode, faces a substrate at the anode. Applying a voltage higher than the breakdown voltage between the cathode and anode ionizes the gas, forming a plasma. Positively charged gas ions are accelerated towards the cathode, and if their energy exceeds the target's surface binding energy, atoms are sputtered away, accumulating on the substrate to form a thin film. Secondary electrons ejected from the target help sustain the plasma by ionizing more gas atoms. Non-inert gases can also be used, leading to reactive sputtering, where sputtered atoms combine with gas molecules to form compound thin films, like nitrides or oxides. The sputtering yield, defined as the number of atoms ejected per incident ion, depends on the ion energy. For energies between 10 eV and 1 keV, the yield is optimal for thin film deposition, while energies above 1 keV are less efficient and can damage the target. The yield decreases as ions penetrate deeper, dissipating more energy as heat [14].

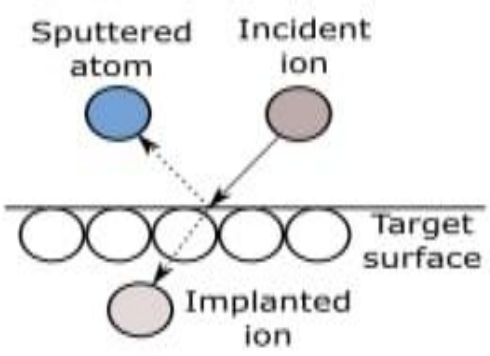

Fig I.11:*The sputtering phenomenon [14]*.

I.5.4 Solar cell equivalent circuit

I.5.4.1 Single diode PV cell modeling

The straightforward model of a solar cell is consists of a current source joint in parallel with a diode as given in **Figure I.12**.

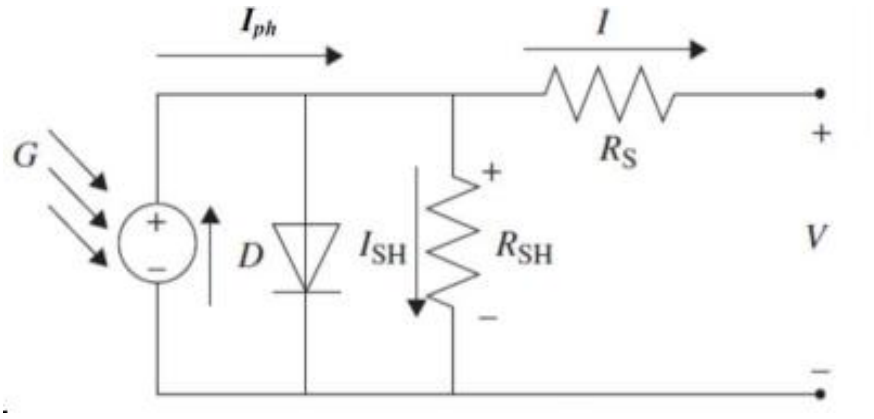

Fig I.12*: Simplest solar cell Equivalent Circuit.*

In the typical solar cell, the Rs=0 and RSH=infinity, thus fails to establish an accurate relationship between cell current and voltage.

In Single diode modeling, a series resistance Rs is considered in order to get precise results. The output current of single diode model is represented as [15]:

$$I=I_{ph}-I_0\left(e^{\frac{q(V+IRs)}{nKT}}-1\right)-\frac{V+IRs}{Rsh} \quad \textbf{(I.4)}$$

By considering the RSH = ∞, the previous equation will be:

$$I=I_{ph}-I_0\left(e^{\frac{q(V+IRs)}{nKT}}-1\right) \quad \textbf{(I.5)}$$

Where:

Iph: photocurrent (A).

Io: reverse saturation current of diode (A).

Rs: series resistance (Ω).

q: electron charges ($1.602x10^{-19}$ C).

T: the temperature of p-n junction (K).

n: diode ideality factor.

k: Boltzmann constant ($1.3806x10^{-23}$) (J/K).

V: cell terminal voltage (V).

I: cell terminal current (A).

A typical **V–I** characteristic of a solar cell is shown in **Figure I.13**.

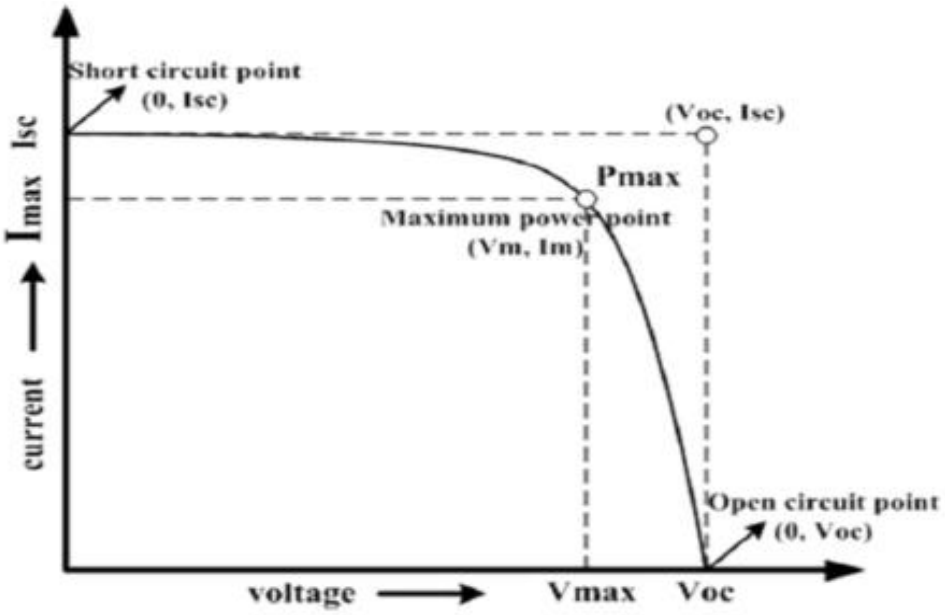

Fig I.13*: I-V characteristics curve of a PV cell [15].*

I.5.4.2 Double diode PV cell modelling

The single diode model provides a satisfactory performance at normal conditions, and has a defect in case of low solar radiation. To overcome this problem, a two diode model is introduced considering two diodes connected in parallel to the current source, shown in **Figure I.14** [15].

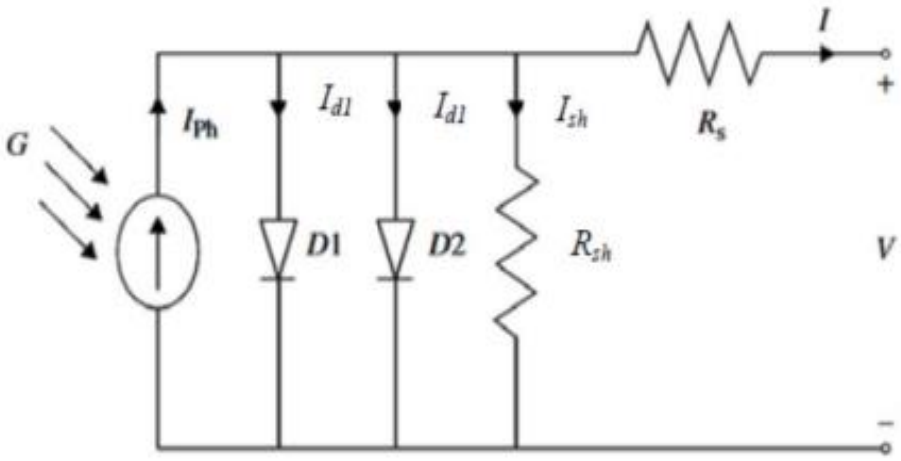

Fig I.14*: Double-diode electrical equivalent circuit of solar cell [15]*.

The current I_{d1}, through the first diode is the current component same as Io in case of single diode model. The current through the second diode I_{d2}, is the recombination current in space charge region. This suggests that two Shockley terms contribute to the saturation currents of a solar PV cell.

Series resistance Rs, and shunt resistance Rp, are same as defined for single diode model. The double diode model of a solar PV-cell is highly accurate at low insolation levels. The double diode model can be represented by the following equation [15].

$$I=I_{PH}-I_{d1}\left(e^{\frac{q(V+IRs)}{n_1KT}}-1\right)-I_{d2}\left(e^{\frac{q(V+IRs)}{n_2KT}}-1\right)-\frac{V+IRs}{Rsh} \quad \textbf{(I.6)}$$

I.5.5 Influence of series resistance and shunt resistance

I.5.5.1 Effect of series resistance variation

The value of series resistance is very small, and in some cases can be neglected. However, to make the model suitable for any given photovoltaic module, it is possible to vary this resistance and predict the influence of its variation on the PV module's outputs. As shown in **Figure I.15**, varying Rs affects the angle of the I-V curve, resulting in a deviation of the slope of the maximum power point [16].

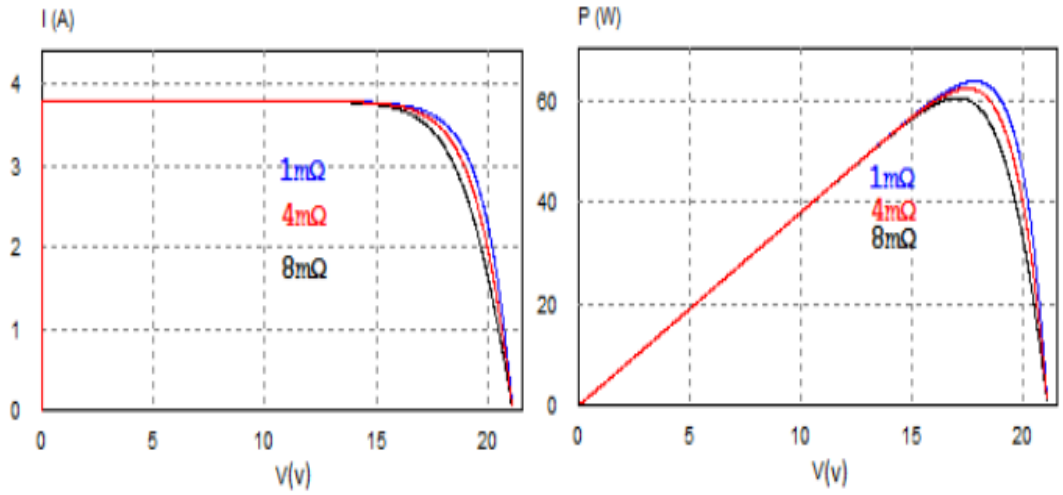

Fig I.15: I-V and P-V curves for different Rs values [16].

I.5.5.2 Effect of shunt resistance variation

The shunt resistance must be sufficiently large for better power output and a good fill factor. Indeed, for a low shunt resistance, the current collapses more strongly, which means that the power loss is high and the fill factor is low (**Figure I.16**) [16].

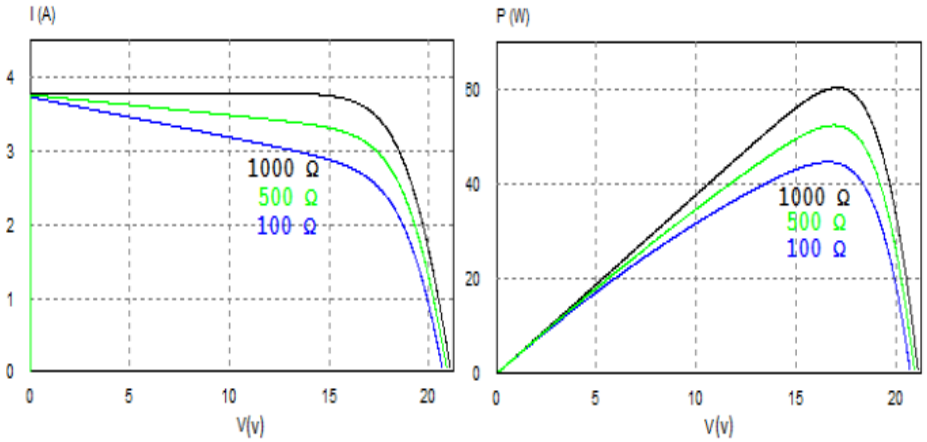

Fig I.16*: I-V and P-V curves for different Rsh values [16]*.

I.5.6 Form factor FF

An important parameter is often used in conjunction with the I(V) characteristic to qualify the quality of a PV cell or generator: the fill factor (FF). This coefficient represents the ratio between the maximum power the cell can deliver (Pmax) and the power formed by the rectangle Icc*Voc. The greater the value of this factor, the greater the exploitable power. The best cells will therefore have undergone technological compromises to achieve the ideal characteristics as far as possible [17].

It is defined by the following relationship:

$$FF=\frac{Pmax}{Vco.Icc} \qquad (I.7)$$

I.5.7 Efficiency η

The efficiency, η of PV cells refers to the power conversion efficiency. It is defined as the ratio between the maximum power delivered by the cell and the incident light power [17],

pin: $$\eta=\frac{Pmax}{Pin}=\frac{FF.Icc.Vco}{Pin} \qquad (I.8)$$

I.6 CONCLUSION

In conclusion, our exploration into the general notions of solar cells has provided a comprehensive understanding of the key components. Beginning with the sun, we recognized its role as an abundant and powerful source of radiation. The study of semiconductors unveiled their pivotal role in converting sunlight into electricity, marking the heart of solar cell functionality.

Moving on to solar cells themselves, our examination covered a different of types, each designed to optimize efficiency and performance in various conditions. From first to third-generation solar cells, we traced the evolution of technology that has significantly improved the quality and effectiveness of solar energy conversionMoreover, we delve into the elaboration methods.

The electric schema governing solar cells was a central focus, emphasizing the intricate process of transforming photons into electrical currents, passing through the mathematical models that govern solar cell configurations, enhancing our ability to analyze, simulate, and improve their performance, to understand the significant impact of series resistance, shunt resistance, as well as the factors influencing the fill factor (FF) and efficiency (η) of solar cells. These parameters collectively shape the performance and effectiveness of solar energy conversion technologies.

CHAPTER II

PEROVSKITE CELL

II.1 INTRODUCTION

With the growing global population and improved living standards, the demand for electricity has surged, placing significant pressure on the planet's resources. Addressing the adverse effects of global warming requires transitioning to renewable energy sources like hydro, wind, and solar power, which can significantly reduce pollution. Solar energy is particularly promising, as the sun provides more energy in a single day than the entire global population consumes in a year.

Among advanced solar technologies, perovskite solar cells (PSCs) have emerged as an innovative option. Unlike traditional silicon-based cells, PSCs consist of materials with a crystal structure similar to the mineral perovskite. These cells have shown remarkable improvements in power conversion efficiency (PCE).

Despite challenges such as efficiency degradation over time, PSCs represent a burgeoning field with immense potential. If researchers can address these issues, PSCs could become strong competitors to traditional silicon solar cells due to their lower cost, flexibility, and ease of production. With increasing investment and research, perovskite solar cells could significantly impact the future of solar energy.

II.2 PEROVSKITE

II.2.1 Perovskite structure

Calcium titanate oxide ($CaTiO_3$) crystal structure is the basic structure of any perovskite material . In 1839 it was first discovered by German mineralogist Gustav Rose in the Ural Mountains, Russia. Later, it is named after Russian mineralist Lev Alekseyevich von Perovski [18].

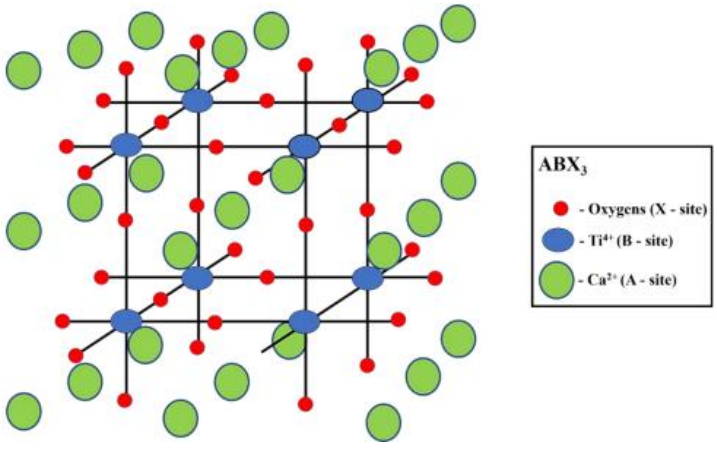

FigII.1*: General perovskite cubic structure.*

ABX_3 is the general perovskite chemical formula for any perovskite compounds, where A is the bigger cation compared to B cation, and X is an anion. In the ideal cubic structure

contains the B cation in 6-fold coordination, which is surrounded by an octahedron of anions, as well as the A cation in 12-fold cuboctahedral coordination demonstrated in **FigureII.1**. The perovskite compoundshave many symmetries, such as cubic, orthorhombic, tetragonal, or trigonal, for examples, $SrTiO_3$, $CaRbF_3$, $FeTiO_3$,$BaTiO_3$,$BiFeO_3$, $PbTiO_3$, etc [19] [20].

II.3 PEROVSKITE SOLAR CELLS

The general formula ABX_3 is used for the 3D organic-inorganic halide perovskites, and the structure is shown in **Figure II.2** Where A is the organic or inorganic cation such as methylammonium ($MA+$), formamidinium ($FA+$), or cesium ($Cs+$), rubidium ($Rb+$), B is a metal anion like lead ($Pb+$) or tin ($Sn+$), and X is halogens such as chloride ($Cl-$), bromide ($Br-$), or iodide (I^-). The various suitable cations and anions are distinguished with their ionic radii value .

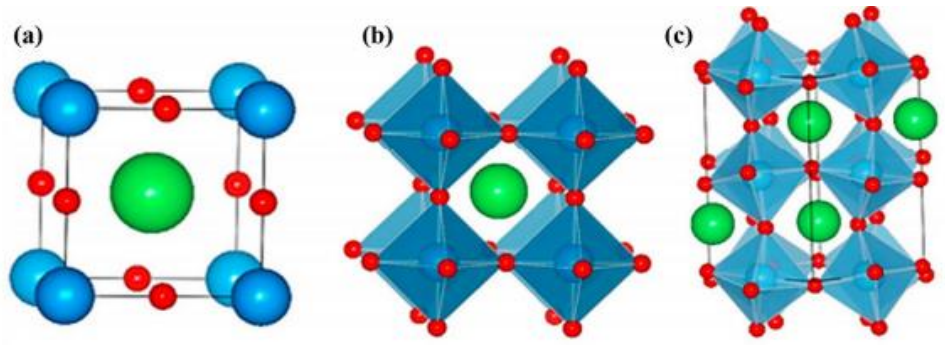

FigII.2*: The generals perovskite cubical crystal structure ABX_3 , where A and B are cations and X is an anion. The anions are bonded to both of the cations [20].*

Perovskite materials, characterized by a crystal structure where cations A and B, along with anions X, form a symmetrical cubic lattice, exhibit diverse properties depending on the composition of these elements. Typically, cation A possesses lower electronegativity and a larger atomic radius compared to cation B, ensuring structural symmetry.

This composition, first discovered by Weber in 1978, typically includes organic components like methylammonium (MA) or formamidinium (FA) as cation A, metals like

lead (Pb) or tin (Sn) as cation B, and halides such as bromide (Br), iodide (I), or chloride (Cl) as anion X [20].

II.3.1 Operation of Perovskite Solar Cells

The PSC operation is described in the schematic shown in figure below.

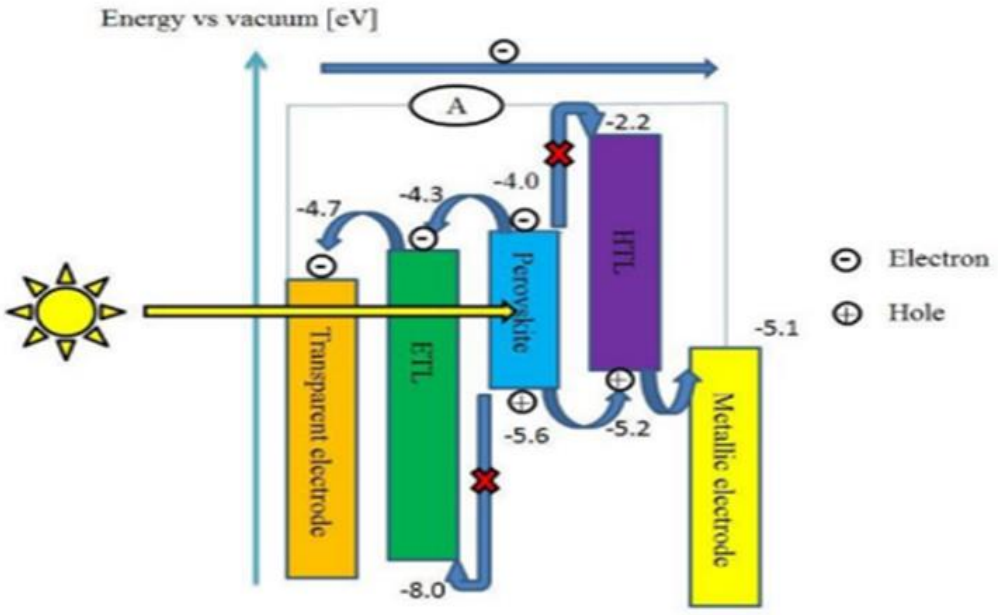

FigII.3*: Schematic energy band diagram showing how perovskite solar cells operate [21].*

Photons from a light source reach the perovskite layer through the glass and transparent electrode. There, they're absorbed, potentially exciting an exciton if the photon's energy exceeds the material's energy gap. This exciton dissociates into free charge carriers due to the potential difference between the transparent and metallic electrodes. Electrons migrate to the electron transport layer (ETL), while holes move to the hole transport layer (HTL). From there, electrons travel to the transparent electrode, generating a current through the wire connecting the electrodes. However, recombination of electrons and holes occurs in the metallic electrode, necessitating careful alignment of energy levels in each layer to minimize this. This is achieved by adjusting the energy levels of the ETL

and HTL relative to the active perovskite layer, ensuring efficient charge carrier transportation and maximizing cell performance [21].

II.3.2 Doping, trap states and defects

Doping is a process used to enhance the conductivity of materials by introducing additional molecules into their structure. By adding molecules with energy levels that align appropriately with the material's existing electronic structure, conductivity can be increased. For instance, molecules with slightly lower highest occupied molecular orbital (HOMO) levels than the material's lowest unoccupied molecular orbital (LUMO) can excite electrons at room temperature, boosting electron conductivity. Conversely, molecules with slightly higher LUMO levels than the material's HOMO can excite electrons, leaving behind holes and thus increasing hole conductivity. Trap states are regions within the material that trap charge carriers and excitons during operation. These trapped charge carriers hinder the flow of current, while trapped excitons require additional energy to be excited. Both scenarios impede the material's overall performance. Defects encompass a range of irregularities within the material, including electrochemical faults, unusual crystal structures, and foreign particles like dust. These defects can disrupt the material's electronic properties and reduce its efficiency [21].

II.3.3 Fabrication of the PSC Devices

Figure II.4 depicts the PSC preparation process.

First: the substrate was etched and cleaned. A wide piece of Teflon tape was applied to one side of a FTO glass substrate. The Teflon tape was subsequently removed, and zinc powder was evenly applied to the surface of the substrate that was not covered by the tape, on which hydrochloric acid was dripped to etch the area through the reaction between the FTO, zinc powder, and hydrochloric acid. Subsequently, the substrate was rinsed using deionized water to remove excess zinc powder and hydrochloric acid and was subjected to ultrasonic agitation in isopropyl alcohol , after which it was dried using nitrogen gas. Teflon tape was subsequently applied to the nonetched area on the opposite side of the substrate , and the substrate was irradiated using a UV-ozone cleaner .

The HTL production method was as follows: the cleaned substrate was placed in a spin coater, and the PEDOT:PSS was coated evenly on it , after which it was heated .

the perovskite active layer was produced through the following procedure: the substrate was cooled to room temperature and placed in a nitrogen atmosphere glove box . The substrate coated with PEDOT:PSS was placed in a spin coater, and perovskite precursor solution was evenly applied to the surface of the substrate through spin-coating, . After the spin-coating was completed, the substrate was moved onto a hot plate and heated . After the substrate had cooled, spincoating of the perovskite active layer was repeated.

The ETL production process was as follows: the substrate coated with the perovskite active layer was placed in a spin coater, and ETL solution was evenly coated onto the surface of the substrate through spin-coating , after which it was removed from the glove box.

Finally, evaporation deposition of the Ag metal electrode was performed. A metal mask was applied to the ETL-coated substrate, which was subsequently placed in the vacuum chamber of a vapor deposition machine, after which the turbine pump was activated and warmed. The duration of evaporation deposition was 4 min, after which the baffle was closed, the current source of the evaporation deposition was turned off, and the vacuum of the chamber was broken to complete PSC device production [22].

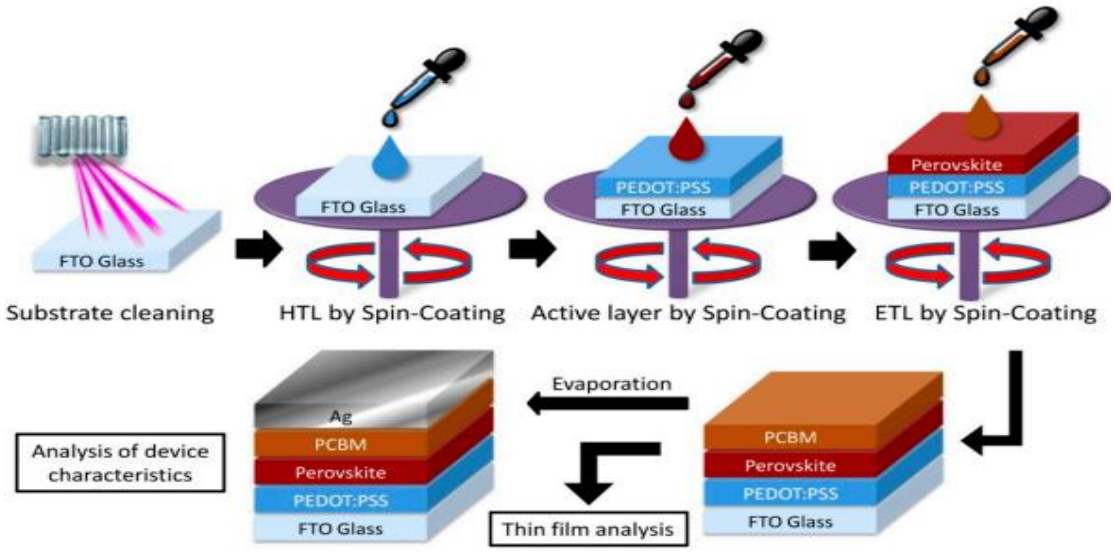

Fig II.4*:The fabrication process of a perovskite solar cell* [22].

II.3.4 Perovskite solar cell device architectures

The device configuration is one of the most crucial factors for evaluating the overall performance of perovskite solar cells. PSCs can be classified as regular (n-i-p) and inverted (p-i-n) structures depending on which transport (electron/hole) material is present on the exterior portion of the cell/encountered by incident light first. These two structures can be further divided into two categories: mesoscopic and planar structures. The mesoscopic structure incorporates a mesoporous layer whereas the planar structure consists of all planar layers [23].

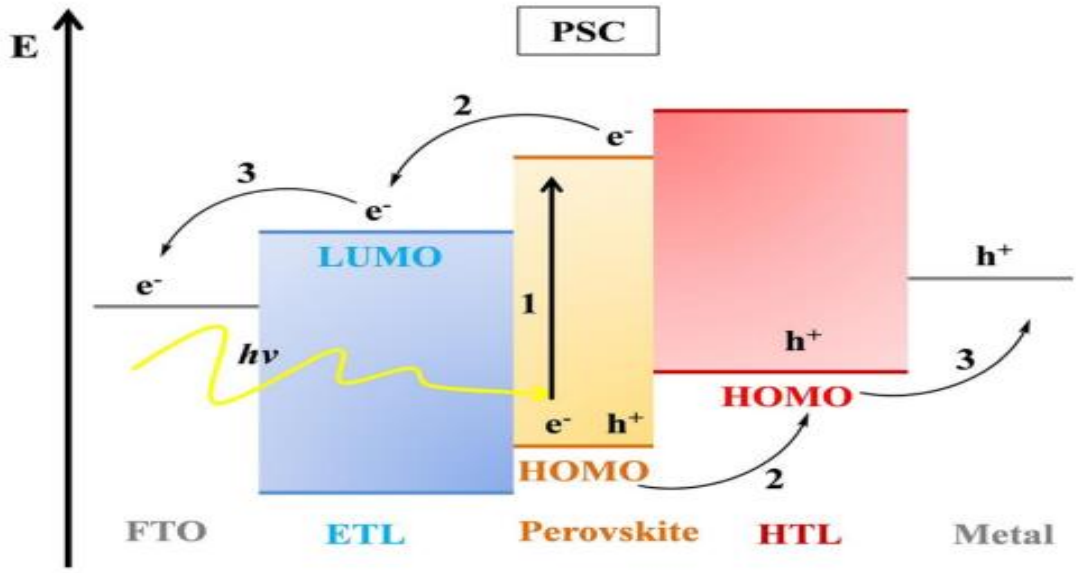

FigII.5*: Band diagram and operation principle of perovskite solar cell.*

Perovskite solar cells without electron and hole-transporting layers have also been tested. In summary, six types of perovskite solar cell architectures have been studied by various researchers thus far: the mesoscopic n-i-p configuration, the planar n-i-p configuration, the planar p-i-n configuration, the mesoscopic p-i-n configuration, the ETL-free configuration, and the HTL-free configuration.

For better understand and optimize solar cells, we use two important equations the Schrödinger equation and the Poisson equation.

The **Schrödinger** equation :

$$\hat{H}\Psi = E\Psi \quad \textbf{(II.1)}$$

$\hat{H}$: Hamiltonian operator

E: Energy eigenvalue

The time-independent equation can be written in any suitable coordinate system, such as Cartesian coordinates (x,y,z). For hydrogenic atoms, spherical polar coordinates are more suitable, hence:

$$\frac{-\hbar^2}{2m}\nabla^2\Psi(r) + V(r)\Psi(r) = E\Psi(r) \quad \textbf{(II.2)}$$

$\frac{-\hbar^2}{2m}\nabla^2\Psi(r)$**:** Kinetic energy

$V(r)\Psi(r)$: Potentiel energy

$E\Psi(r)$: Total energy

$\hbar$:the reduced Planck constant,
m : the electron mass,
∇ : the Laplacian operator,
Ψ: the wave function,
V : the potential energy,
E**:** the energy eigenvalue,
(r) :denotes the quantities are functions of spherical polar coordinates (r, θ, φ)

The **Poisson** equation:

it is crucial in the field of solar cells for modeling the electrostatic potential within the device:

$$\nabla^2\phi(r) = -\frac{\rho(r)}{\epsilon} \quad \textbf{(II.3)}$$

$\phi(r)$: the electrostatic potential.

$\rho(r)$: the charge density.

ϵ : the permittivity of the material.

II.3.5 Solar cells based on perovskites

In perovskite solar cell engineering, there are two main classes: n-i-p structured devices and p-i-n structured ones, as illustrated in **Figure II.6**. The temporal order in which the layers of the solar system are deposited creates this group difference. The n-i-p structuring starts with the ETL (a type n material), followed by the perovskite layer (an almost intrinsic i material), and ends with the HTL (a type p material); the reverse order is true for the p-i-n structure. The role of each layer remains the same in both classes, where the perovskite layer generates charge carriers (electrons and holes), which are then transferred to the ETL for electrons and the HTL for holes before being collected by the electrodes (cathode and anode respectively) [24].

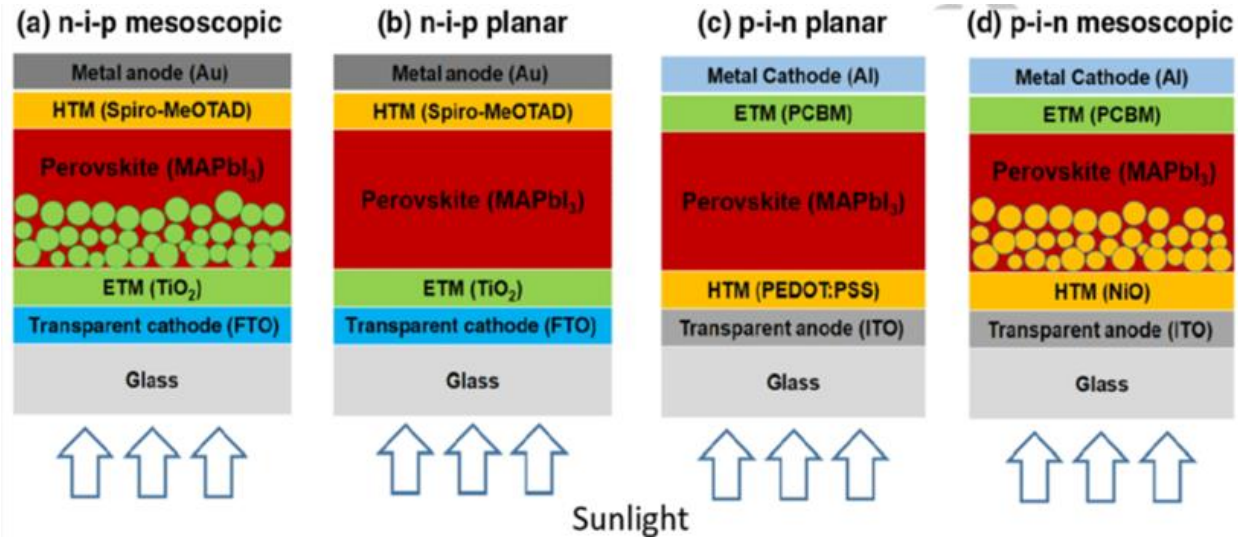

FigII.6*:Diagram of the two structures (n-i-p type on the left and p-i-n type on the right) as well that of the two architectures (planar or mesoporous) achievable for the development of cells solar perovskites.*

Two other different architectures have emerged and been adopted, such as mesoporous or planar (**Figure II.4**). The former relies on a substrate-side base (i.e., ETL in n-i-p and HTL in p-i-n) consisting of two parts, one compact and the other mesoporous. The latter relies solely on a compact base. The mesoporous architecture has been adopted from dye-sensitized solar cells, from which perovskite solar cells emerged [25]. As a result, porous perovskite cells with n-i-p structure first appeared in 2009. Later, the first perovskite p-i-n cell was reported in 2013, leading to the emergence of planar perovskite cells [26].

Thus, the development of photovoltaic devices has extended to planar perovskite solar cells with n-i-p structure and porous perovskite solar cells with p-i-n structure (less common), as presented in the figure II.6. There are developments of cells without HTL in the photovoltaic literature. (with a carbon paste electrode) that are particularly interesting in their manufacturing method. Sometimes, photovoltaics are devoid of ETL, but their efficiency remains very low [27]. Frequently, n-i-p perovskite cells outperform p-i-n ones. The earlier development of the former and the generally adopted mesoporous architecture in this case reinforce this advantage. However, both structures are interesting and lead to high efficiencies of up to over 20%, whether in mesoporous or planar architecture [28]. However, the planar architecture seems more appealing due to its simplicity of implementation since it uses lower temperatures. This criterion is also more adopted in the development of flexible perovskite devices because it is compatible with flexible substrates like Polyethylene terephthalate (PET). This is equally the case for the development of tandem cells, where the lower sub-cell requires low fabrication temperatures to prevent degradation.

II.3.6 Interface architecture

The performance of perovskite solar cells heavily depends on the materials used at the interfaces (HTL and ETL), impacting efficiency. These materials should minimize light absorption to prevent energy loss and facilitate charge transport. They should also have energy levels aligned with the perovskite to ensure efficient charge transfer while blocking reverse charges. Maintaining a balance in hole and electron transport is crucial for optimal charge collection. Additionally, energy alignment significantly affects the open-circuit voltage(Voc) of the device.

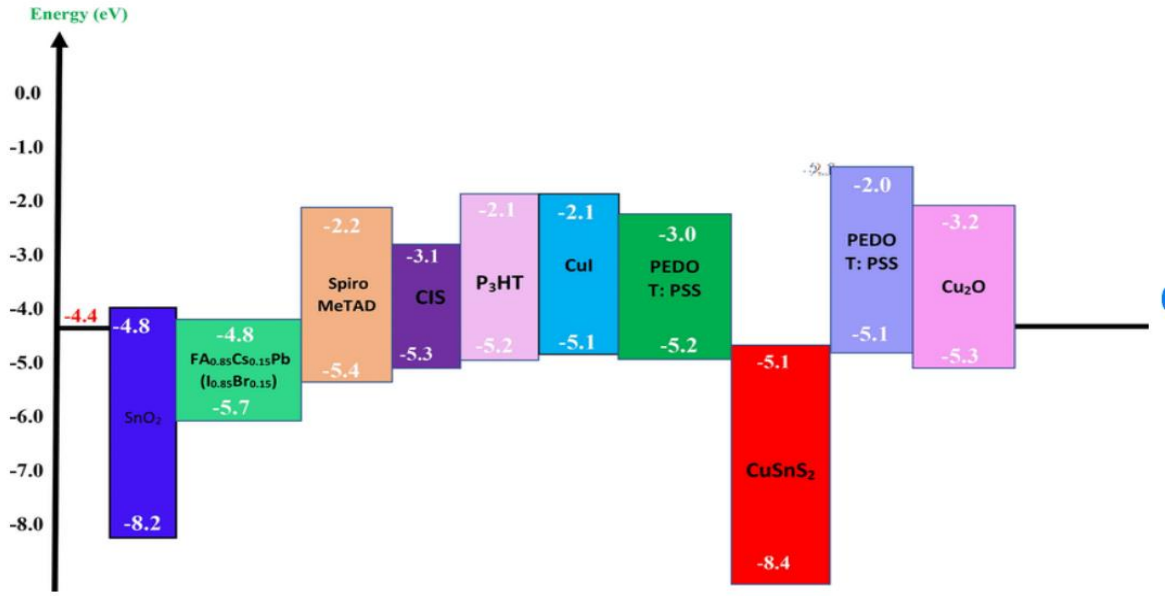

FigII.7*: Energy diagram of ETL, HTL and perovskite active layer [29].*

The open-circuit voltage is also affected by defects or electronic traps, especially at the interfaces with perovskite, which consequently impacts the efficiency of solar cells. The density of traps can vary considerably depending on the interface material used. This introduces a criterion of adaptation and stability between the interface material and the perovskite that ideal HTL and ETL must meet by minimizing the formation of these types of traps. In all interface materials, there are several categories in which they are grouped. Although there are many variations and nuances within the same category, they can be distinguished as follows: metal oxides, organic materials (small molecules, SAM molecules, and polymers), and carbon-based materials (mainly fullerenes) Metal oxides are generally more stable than organic oxides; however, they are sometimes limited to solid substrates, negatively influencing performance [30].

II.3.7 Hole Transport Layers (HTL) and HTL/Perovskite Interface

The organic material commonly used as HTL in perovskite n-i-p photovoltaics is Spiro-OMeTAD, preferred for its advantageous characteristics such as simplicity in fabrication and effectiveness in PV cells. However, it has negative properties such as instability over time and susceptibility to light-induced porosity [31]. In contrast to organics, inorganic materials can be employed as HTL. Among various available metal oxides (particularly nickel and copper-based), NiO2 is more prevalent due to its higher performance. To enhance its performance, optimizations through additives can be implemented in the NiO layer, primarily including Li and Mg.Indeed, interface engineering involves optimizing interfaces, in this case, between the HTL and perovskite layer to limit recombination, thus gaining in Voc and FF, enhancing selectivity, transfer, and collection of charge carriers, resulting in gains in Jsc and FF. Various approaches are designated, primarily involving oxygen plasma treatments performed before the deposition of the perovskite layer, specifically in the p-i-n structure. Other surface treatments exist, notably applied directly to the perovskite layer once formed in the case of the n-i-p structure. Generally, such treatments help limit the density of electronic traps by passivating the perovskite surface, thereby improving the electrical quality of the interface [32].

II.3.8 Electron Transport Layers (ETL) and Perovskite/ETL Interface

Metal oxides are commonly used as electron transport layers (ETL) in perovskite photovoltaics. TiO2 is widely employed due to its compatibility with perovskite devices, especially in mesoporous form, and its recent achievement of world-record efficiencies [33]. However, TiO2 fabrication requires high temperatures, making it costly, and its sensitivity to UV light can cause instability in perovskite layers. Tin oxide (SnO_2) is an alternative ETL material known for its transparency, intrinsic stability, and excellent electrical properties. SnO_2 has demonstrated efficiencies exceeding 20% in various studies and offers advantages such as compatibility with perovskite, reduced hysteresis, and lower fabrication temperatures compared to TiO_2. Zinc oxide (ZnO) is also utilized but tends to result in lower performance due to its instability when in contact with perovskite [34] [35].

ZnO instability can be mitigated through thermal annealing or passivation of surface defects. Aluminum additives improve the performance of ZnO-based ETLs, but instability issues persist. Additionally, organic materials like fullerenes (C60 and derivatives) are used for their excellent electron extraction and transport properties. However, fullerenes may have poor charge selectivity and require additional layers to address interface issues. Overall, metal oxides offer promising avenues for improving the efficiency and stability of perovskite solar cells, with ongoing research exploring new materials and optimization strategies [36].

II.3.9 Advantages of Perovskite solar cells

- **Low cost and ease of manufacturing**: Perovskites hold the promise of being a low-cost technology with great ease of manufacture and decreased capital expenditure.
- **Tunable bandgap**: the bandgap of perovskite solar cells can be modified through control of the composition of the perovskite material.
- **High applicability**: perovskite materials can absorb wide wavelengths of light, which makes them suitable for unique applications (Agrivoltaics), tandem (to complement Silicon or other PV materials) and to be placed in places where silicon PVs do not function well (indirect lighting, indoor, low sun angles, etc.).
- **Efficiency**: perovskite-based solar cells are showing an impressive rise in efficiency over in the last decade (recent studies have even passed 30%), and hopefully will allow for high-performance, low-cost PVs.
- **Low weight** (when produced on plastics, compared to glass-based silicon PVs)
- **Flexible form factors**: since perovskite materials can be solution-processable, they can be printed or painted over flexible surfaces and enable solar windows, entire rooftops and more.
- **Transparency**: perovskite materials can enable transparent panels that can be integrated into buildings (BIPV) or other devices.
- **Sustainability**: soluble production processes are highly efficient in terms of energy and material waste
- **Recyclability**: most perovskite panels are highly recyclable, some reaching a 100% recyclability rate.
- **Abundant and low-cost materials**: Perovskites rely on stable and abundant resource materials, such as methylammonia, lead, and iodine.
- Very high **return on investment** (in terms of Watts/$) [37].

II.3.10 Disadvantages of Perovskite solar cells

Nontoxic tin-based perovskite solar cells (PSCs) have attracted attention, but are easily oxidized, which causes their performance and stability to be far behind lead-based PSCs. Here, strategies to improve the stability of tin-based PSCs (additive engineering, deoxidizer, partial substitution, and reduced dimensions) are reviewed. Outlooks are also proposed to avoid the shortcoming for fabricating highly efficient and stable PSCs [38].

II.4 $FASnI_3$

Formamidinium tin triiodide ($FASnI_3$) is a suitable candidate for the absorber layer in perovskite solar cells (PSC) because of its non-toxicity, narrow band gap, thermal stability and high carrier mobility. This study focuses on the analysis and improvement in the performance of $FASnI_3$-based PSCs using various inorganic charge transport materials [39].

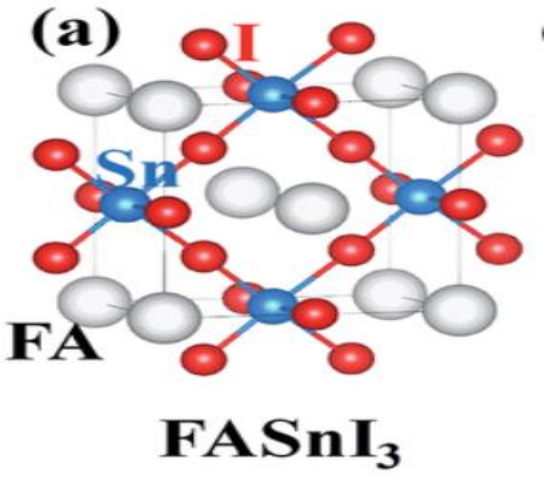

FigII.8*: The schematic perovskite structure of $FASnI_3$ [39].*

II.4.1 Properties of FASnI3 for Perovskite Solar Cells

The FA cation is slightly larger than MA and can also be an A-site cation in Sn-based perovskites. $FASnI_3$ adopts an average cubic $Pm\bar{3}m$ crystal structure with lattice parameter being a = 6.3290(9) Å or alternatively the pseudocubic, orthorhombic structure.

The band gap of $FASnI_3$ film is about 1.41 eV, which is wider than that of $MASnI_3$ film and narrower than that of Pb-based perovskites.

Lee et al. found that the introduction of bromide into $FASnI_3$ lattice significantly lowers the carrier density of perovskite absorber, arising from the reduction of Sn vacancies. Therefore, it can reduce leakage current, increase recombination lifetime, and lead to an enhanced and reproducible the device performance. Synthesis, resistivity, and thermal properties of the cubic $FASnI_3$ perovskite were first investigated in 1997. $FASnI_3$ has similar thermal stability but lower conductivity, compared with $MASnI_3$.

first demonstrated that $FASnI_3$ based solar cells with the incorporation of SnF_2 achieved a PCE of 2.1%. Most recent high-performance Sn-based perovskite solar cells are mainly based on $FASnI_3$ materials,because of their better air stability than that of $MASnI_3$. Dang et al. compared the properties of bulk $MASnI_3$ and $FASnI_3$ single crystals and found that they are p-type and n-type semiconductors, respectively, with trap densities as low as ~1011 cm^{-3} . Their results confirmed that the air-stability of $FASnI_3$ crystals is much better than that of $MASnI_3$ crystals. The degradation mechanism of Sn halide perovskites studied by Wang et al also confirmed that $FASnI_3$ has a better tolerance for O_2. The results were investigated by chemical analyses and theoretical calculations. It was found that, in $MASnI_3$, Sn^{2+} can be easily oxidized to Sn^{4+} and replacing MA with FA can reduce the extent of Sn oxidation. Moreover, $FASnI_3$ film exhibits a lower conductivity than $MASnI_3$.

studied the effects of A-site cations on the defect physics of Sn halide perovskites and found that the organic cations, i.e., FA and MA, play a vital role. DFT calculations showed that the antibonding overlap between Sn-5s and I-5p orbitals is clearly weaker in $FASnI_3$ than in $MASnI_3$ because of the larger ionic size of FA, leading to higher formation energies of Sn vacancies in $FASnI_3$.

The conductivity of $FASnI_3$ can be tuned from p-type to intrinsic by varying the growth conditions, while $MASnI_3$ can only show unipolar high p-type conductivity. Those results provide a reasonable explanation for the better performance and stability of $FASnI_3$-based solar cells with respect to the $MASnI_3$ cells. Therefore, $FASnI_3$ is an excellent absorber candidate for Pb-free perovskite solar cells. In addition to solar cells, Milot et al. suggested that $FASnI_3$ perovskite is highly suited to lightemitting devices. The $FASnI_3$ material exhibits a threshold charge-carrier density of 8×1017 cm^{-3} and a charge-carrier mobility of 22 cm^2 $V^{-1}.s^{-1}$. Furthermore, the $FASnI_3$ has strong radiative bimolecular recombination and Auger rates that are over an order of magnitude lower than Pb analogs [40].

II.5 RECOMBINATION

Any electron which exists in the conduction band is in a meta-stable state and will eventually stabilize to a lower energy position in the valence band. When this occurs, it must move into an empty valence band state. Therefore, when the electron stabilizes back down into the valence band, it also effectively removes a hole. This process is called recombination. There are three basic types of recombination in the bulk of a single-crystal semiconductor.

II.5.1 Radiative (Band-to-Band) Recombination

Radiative recombination is the recombination mechanism that dominates in direct bandgap semiconductors. The light produced from a light emitting diode (LED) is the most obvious example of radiative recombination in a semiconductor device. Concentrator and space solar cells are typically made from direct bandgap materials (GaAs etc) and radiative recombination dominates. However, most terrestrial solar cells are made from silicon, which is an *indirect* bandgap semiconductor and radiative recombination is extremely low and usually neglected. The key characteristics of radiative recombination are :

- In radiative recombination, an electron from the conduction band directly combines with a hole in the valence band and releases a photon; and

- The emitted photon has an energy similar to the band gap and is therefore only weakly absorbed such that it can exit the piece of semiconductor [41].

  For radiative recombination coefficient, the equation used is:

$$\mathbf{Br} = \frac{\mathbf{1}}{(\boldsymbol{\tau}\mathbf{p,rad} \times \mathbf{NA})} \quad \textbf{(II-4)}$$

$$\mathbf{Br} = \frac{\mathbf{1}}{(\boldsymbol{\tau}\mathbf{n,rad} \times \mathbf{Nd})} \quad \textbf{(II-5)}$$

Br: represents the radiative recombination coefficient in cm3/s.

τp,rad : radiative lifetimes of the hole minority carrier.

τn,rad: radiative lifetimes of the electron minority carrier.

NA,ND :the doping densities.

II.5.2 Recombination Through Defect Levels

Recombination through defects, previously known as Shockley-Read-Hall (SRH or RHS) recombination, occurs via a trap level or defect energy level in the band gap. Defect recombination is a two-step process:

- An electron (or hole) is trapped by an energy state in the forbidden region which is introduced through defects in the crystal lattice. These defects can either be unintentionally introduced or deliberately added to the material, for example in doping the material; and
- If a hole (or an electron) moves up to the same energy state before the electron is thermally re-emitted into the conduction band, then it recombines.

The rate at which a carrier moves into the energy level in the forbidden gap depends on the distance of the introduced energy level from either of the band edges. Therefore, if an energy is introduced close to either band edge, recombination is less likely as the electron is likely to be re-emitted to the conduction band edge rather than recombine with a hole which moves into the same energy state from the valence band. For this reason, energy levels near mid-gap are very effective for recombination [42].

II.5.3 Auger Recombination

Auger Recombination involves three carriers. An electron and a hole recombine, but rather than emitting the energy as heat or as a photon, the energy is given to a third carrier, an electron in the conduction band. This electron then thermalizes back down to the conduction band edge.

Auger recombination is most important at high carrier concentrations caused by heavy doping or high level injection under concentrated sunlight. In silicon-based solar cells (the most popular), Auger recombination limits the lifetime and ultimate efficiency. The more heavily doped the material is, the shorter the Auger recombination lifetime [43].

for Auger recombination coefficients, the equation is:

$$\mathbf{B_{Auger,n,P}} = \frac{1}{(\tau porn,Auger \times NAorND)} \qquad \textbf{(II-5)}$$

In this equation, BAuger,p and BAuger,n denote the Auger recombination coefficients for holesand electrons, respectively.

II.6 CHARGE TRANSFER MECHANISMS

Three types of charge transfer mechanisms occur when two semiconductors interface with one another. In a type (I) heterojunction, both electrons and holes from semiconductor I (SCI) recombine with those of semiconductor II (SCII) due to the more positive conduction band (CB) and less positive valence band (VB) of SCII compared with SCI, respectively. When the CB of SCI is more negative than that of SCII and when the VB of SCII is more positive than that of SCI, a type (II) heterojunction is formed where electrons and holes are correspondingly transferred towards SCII and SCI. In both type (I) and type (II) heterojunctions, electrons and holes move towards lower energy potentials where reduction and oxidation occur, respectively. When band positions are further set off, a broken gap is formed where electrons/holes are excluded from participating in the (reduction/oxidation) redox reaction, regarded as a type (III) heterojunction (**FigureII.10**). In all the aforementioned heterojunction types, a spatial charge transfer is generated that enhances the separation of electron/hole pairs due to internal electric . Band bending at the interface can also facilitate electron transfer from one semiconductor to another. Moreover, electrolyte redox reaction occurs only when a

semiconductor possesses carriers with higher energy than the electrolyte thermodynamic potential.For photocatalysts, therefore, the energy band position of two semiconductors is arguably the only parameter affecting the charge transfer [44].

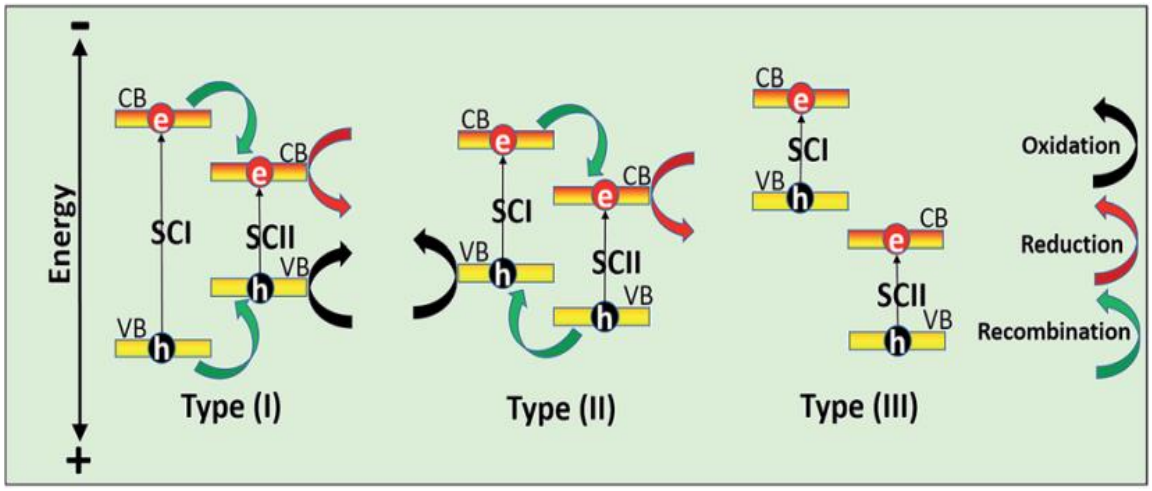

FigII.9*: Three types of charge transfer mechanisms.*

II.7 CONCLUSION

In conclusion, our exploration of perovskite solar cells has unveiled a promising frontier in the realm of photovoltaics, marked by both remarkable advancements and lingering challenges.we meticulously examined the advantages and disadvantages of perovskite solar cells. We marveled at their high efficiency, cost-effectiveness, and versatility, envisioning a future where perovskite-based technologies play a pivotal role in meeting our growing energy demands sustainably. However, we also confronted the formidable obstacles that stand in the path of widespread adoption, including stability issues, material toxicity, and environmental concerns.Amidst this intricate landscape, the emergence of Formamidinium Tin Triiodide ($FASnI_3$) presents a glimmer of hope. This eco-friendly perovskite variant offers a compelling solution to some of the environmental drawbacks associated with traditional perovskite materials. Its compatibility with nature holds the promise of mitigating ecological impacts, fostering a more sustainable approach to solar energy harnessing.Yet, we cannot overlook the persistent challenge of oxidation, which poses a significant threat to the stability and longevity of $FASnI_3$-based solar cells. In essence, our exploration of perovskite solar cells is a testament to the relentless pursuit of clean, renewable energy solutions.

CHAPTER III

SIMULATION OF THE $FASnI_3$ SOLAR CELL

III.1 INTRODUCTION

In this chapter, we explore the simulation and optimization of perovskite solar cells (PSCs) based on formamidinium tin iodide ($FASnI_3$). Using the SCAPS software, a powerful tool for simulating thin-film solar cells, we aim to enhance the efficiency of these lead-free PSCs. The process involves setting up the device structure in SCAPS, inputting the material properties, and systematically varying key parameters to find the optimal configuration. Our goal is to understand how different factors affect the performance of $FASnI_3$-based PSCs and to identify the best setup for achieving the highest efficiency.

III.2 MATERIALS AND METHODS

III.2.1 Solar cell architecture and parameters of simulations

Figure III.1 and **Figure III.4** illustrates the hetero-structure perovskite solar devices used in our simulations. Those solar devices consist of several layers:

Structure 1: FTO/ n-type FASnI3 (ETL)/i-type $FASnI_3$/p-type $FAGeCl_3$ (HTL)/Au.

Structure 2: FTO/ n^+-$FASnI_3$/n-type $FASnI_3$ (ETL)/i-type $FASnI_3$/p-type $FAGeCl_3$ (HTL)/Au.

Numerical simulations were conducted using the SCAPS-1D software. The simulations were based on a solar spectrum of AM 1.5 with an incident power density of 100 mW/cm^2 and the operating temperature of the cell was 300 K [1].

To accurately simulate the perovskite solar cell, we compiled a set of key physical parameters as shown in Table III.1. This data, summarized in Table, includes properties such as layer thicknesses, carrier densities (both acceptor, NA, and donor, ND), the material's band gap energy (Eg), its electron affinity, and the relative permittivity, the mobilities of both electrons (μn) and holes (μp) were incorporated, along with information about defect densities within the material.

Additionally, the study considered interfacial defects as listed in Table III.2:

Structure 1: HTL/absorber, absorber/ETL, and ETL/FTO.

Structure 2: HTL/absorber, absorber/ETL, ETL/ n^+-$FASnI_3$ and n^+-FASnI3/FTO.

III.3 PARAMETERS OF THE STUDIED PEROVSKITE CELL

Table III.1:Properties of the different layers of the solar cell (FTO, n-$FASnI_3$ (ETL), i-$FASnI_3$ (absorber), n^+-$FASnI_3$, p-$FAGeCl_3$ (HTL) [1], [2].

Parameter	FTO	n^+-$FASnI_3$	n-$FASnI_3$ (ETL)	i-$FASnI_3$ (absorber)	p-$FAGeCl_3$ (HTL)
Ban gap (eV)	3.5	1.36–1.44	1.4	1.4	3.34
Thickness (nm)	500	800	70	800	300
Electron affinity X (eV)	4	4.17	4.17	4.17	2.45
Relative permittivity	8.2	8.2	8.2	8.2	3
CB effective DOS (cm^3)	2.2×10^{18}	10^{18}	10^{18}	10^{18}	2.500×10^{18}
CB effective DOS (cm^3)	2.2×10^{18}	10^{18}	10^{18}	10^{18}	1.800×10^{19}
electron/Hole thermal velocity (cm/s)	10^7 / 10^7	10^7 / 10^7	10^7 / 10^7	10^7 / 10^7	10^7 / 10^7
Mobility of electron/hole µe/µh(cm^2 / Vs)	20/20	22/22	22/22	22/22	$2 \times 10^{-4}/2 \times 10^{-4}$
Donor density ND (cm^{-3})	2.10^{19}	10^{18}	10^{18}	0	0
Acceptor density NA (cm^{-3})	0	0	0	7.10^{16}	10^{19}
Density of defects	10^{15}	10^{15}	10^{15}	10^{15}	10^{15}
Transmission (%)	60				

Table III.2:The interfacial-defects parameters between HTL/ ($FAGeCl_3$) absorber, ($FASnI_3$) absorber/ ($FASnI_3$) ETL and ($FASnI_3$) ETL/FTO [1].

	HTL/ Absorber	Absorber/ ETL	ETL/ FTO
Defect type	Neutral	Neutral	Neutral
Capture cross section for electron (cm^2)	10^{-19}	10^{-19}	10^{-19}
Capture cross section for hole (cm^2)	10^{-19}	10^{-19}	10^{-19}
Energetic distribution	Single	Gaussian	Single
Energy level with respect to eV	0.6	0.6	0.6
Characteristic energy (eV)		0.1	
Total density (cm^3)	10^{14}	10^{14}	10^{14}

III.4 SIMULATIONS RESULTS

III.4.1 Structure 1

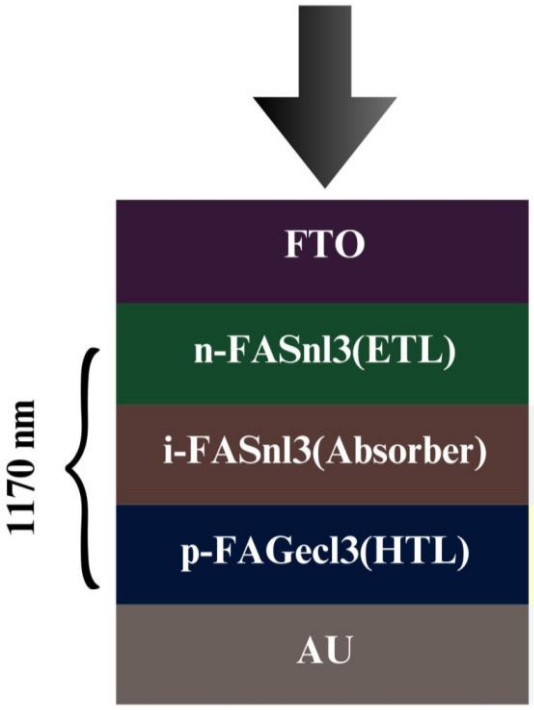

***Fig III.1**: Illustration of the architecture of the simulated PSC.*

Fig III.1 shows the structure of the perovskite solar cell based on $FASnI_3$ that we are going to simulate. This cell consists of the layers: FTO/ n-type $FASnI_3$ (ETL)/i-type $FASnI_3$/p-type $FAGeCl_3$ (HTL)/Au.

III.4.1.1 Simulation of the studied perovskite cell

The simulation results for the various layers of the solar cell (FTO/n-$FASnI_3$, i-$FASnI_3$/p-$FAGeCl_3$, Au) include key outputs such as I-V characteristics, quantum efficiency (QE), efficiency, VOC, JSC, and (FF), which are presented in the following figures.

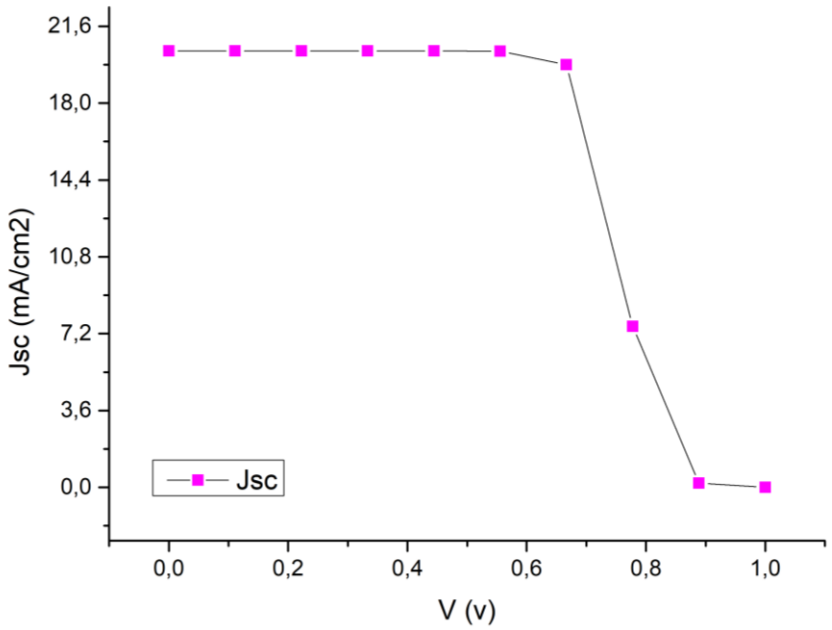

Fig III.2: *J-V Characteristic graph.*

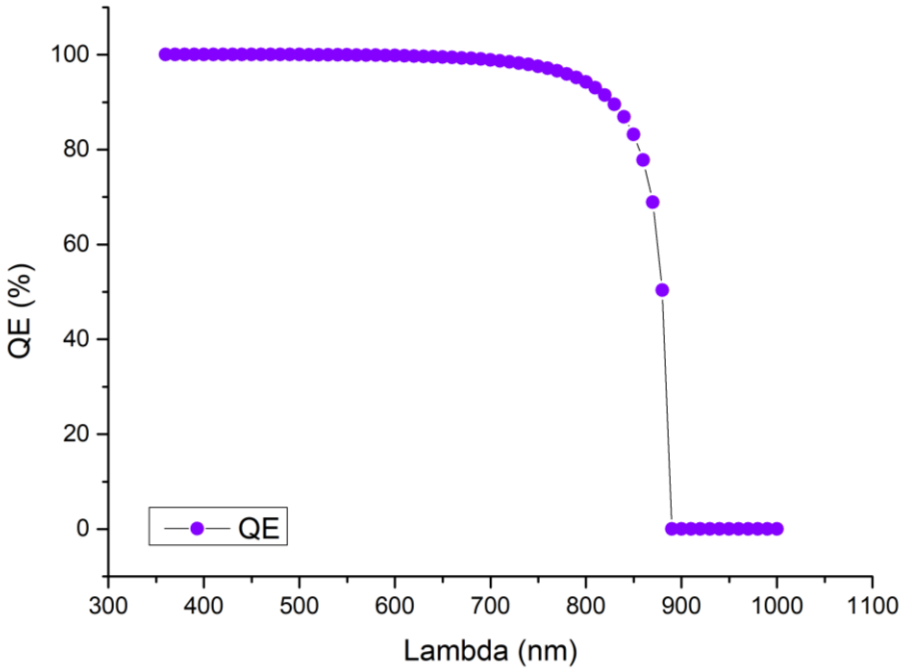

Fig III.3*: QE in terms of Lambda.*

Table III.3: Represent the result of the simulation of the studied perovskite cell efficiency, VOC, JSC, FF,eta.

Solar cell architecture	Voc(V)	Jsc (mA/ cm2)	FF (%)	PCE (%)
	1.001805	**20.44403526**	**64.8287**	**20.4187**

The simulation's results, presented in the **Table III.3**, provide valuable data. We've identified an opportunity to improve performance by incorporating a new layer, n+-$FASnI_3$, hoping to achieve a significant enhancement in overall efficiency.

III.4.2 Structure 2

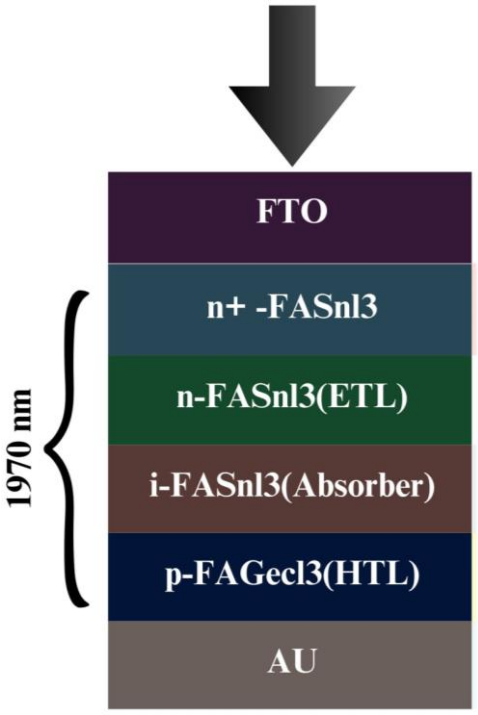

Fig III.4*: Illustration of the architecture of the simulated PSC (with n+-FASnI₃ layer).*

Fig III.4 shows the structure of the perovskite solar cell based on $FASnI_3$ that we are going to simulate. This cell consists of the layers: FTO/ n-type $FASnI_3$ (ETL)/i-type $FASnI_3$/ n+-$FASnI_3$/p-type $FAGeCl_3$ (HTL)/Au.

III.4.2.1 Simulation of the studied perovskite cell

We introduced an additional interfacial defect between the n+-FASnI3 layer and the electron transporting layer (ETL). This defect shares the same properties as the other interfacial defects.

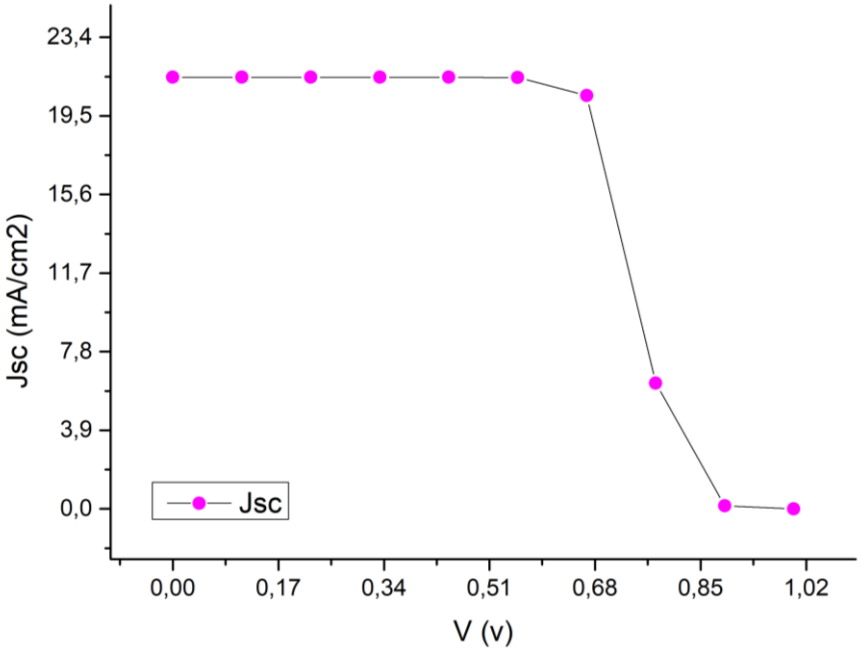

Fig III.5*: J-V Characteristic graph (with n^+-$FASnI_3$ layer).*

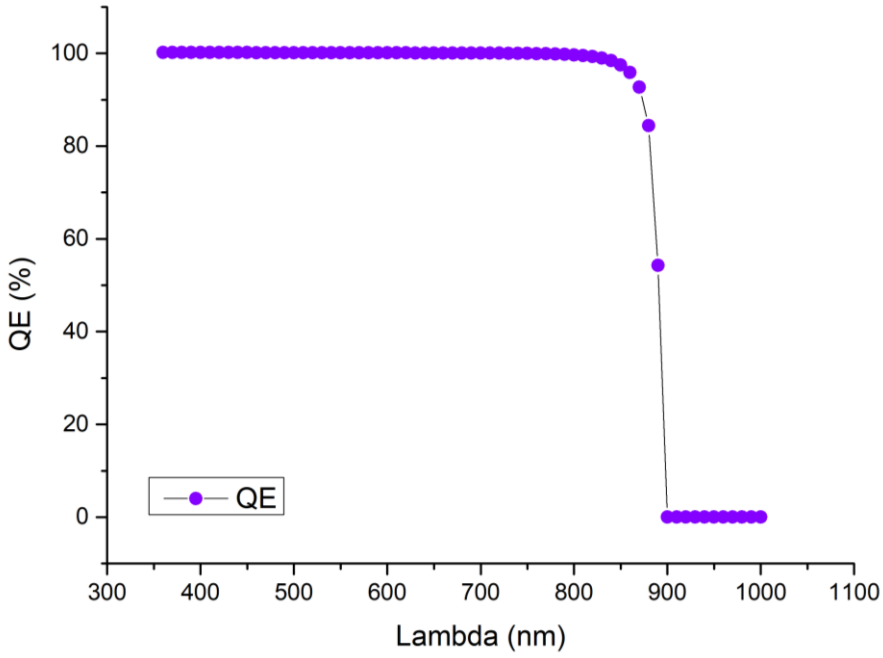

Fig III.6*: QE in terms of Lambda (with n^+-$FASnI_3$ layer).*

Table III.4: Represent the result of the simulation of the studied perovskite cell with n^+-$FASnI_3$ (VOC, JSC, FF,eta).

Solar cell architecture	Voc(V)	Jsc (mA/ cm2)	FF (%)	PCE (%)
	1.001793	21.41760439	63.8561	21.0699

The performance data from the simulation, detailed in **Table III.4**, provides a clear picture of the impact of the newly added layer (n^+-$FASnI_3$). As anticipated, the results demonstrate a significant improvement in performance compared to the initial structure. This successful optimization validates our design choices and paves the way for further refinement.

III.5 RESULTS AND DISCUSSION

The addition of the n^+-$FASnI_3$ ayer led to promising improvements in device performance. To understand how this layer interacts with the existing structure, we investigated the effects of carrier concentration and thickness on the other functional layers (n-$FASnI_3$ (ETL)/i-$FASnI_3$/p-$FAGeCl_3$ (HTL)). By analyzing these interactions, we aim to optimize the entire device architecture and unlock its full potential.

III.5.1 Influence of the thickness and doping level of absorber layer

In perovskite solar devices, the thickness of the active material plays a crucial role in determining both the quality of the perovskite layer and the overall device performance, particularly in maximizing current density. This thickness significantly influences the diffusion length of charge carriers. A thinner absorber layer, while beneficial for some properties, leads to reduced absorption and subsequently lowers the photocurrent and overall efficiency of the device. On the other hand, an excessively thick absorber layer may hinder charge carriers from effectively reaching the charge-collecting materials, resulting in increased series resistance and reduced solar cell efficiency [1].

The i-FASnI3 absorber thickness and doping level were varied between 100 nm to 1600 nm and 10^{14} cm^{-3} to 10^{18} cm^{-3}, respectively. The following figures illustrates the influence of these variations on the device's photovoltaic performance. As the thickness of the absorber layer increases, the power conversion efficiency (PCE) also increases, a high PCE of 21.39% and 20.97% is achieved For a doping level of 9.3e14 cm^{-3} and a thickness of 1590 nm, respectively.

Both the PCE and short-circuit current density (Jsc) increase with the absorber thickness, reflecting a higher rate of electron-hole pair generation[1].The graph clearly shows that the highest Jsc values correspond to regions with greater absorber thickness. When the thickness of i-$FASnI_3$ increases from 100 nm to 1600 nm, Jsc rises from 20.81 mA/cm^2 to 21.30mA/cm^2, resulting in increased absorption of longer wavelength photons [1].

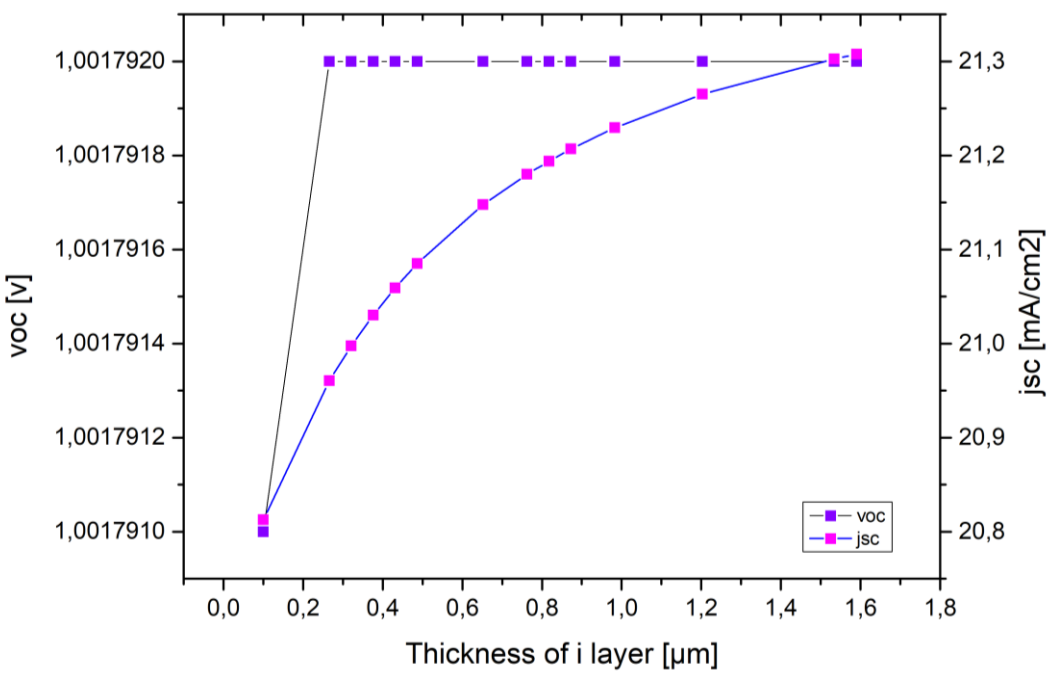

Fig III.7: *The impact of the thickness of i-layer on the device performances (Voc,Jsc).*

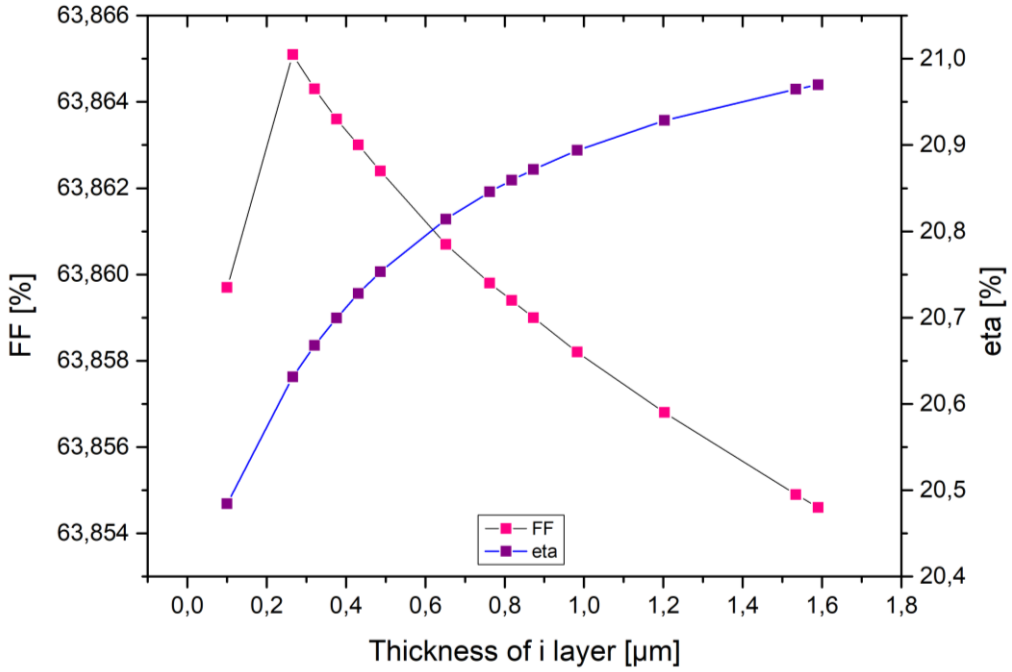

Fig III.8: *The impact of the thickness of i-layer on the device performances (FF,eta).*

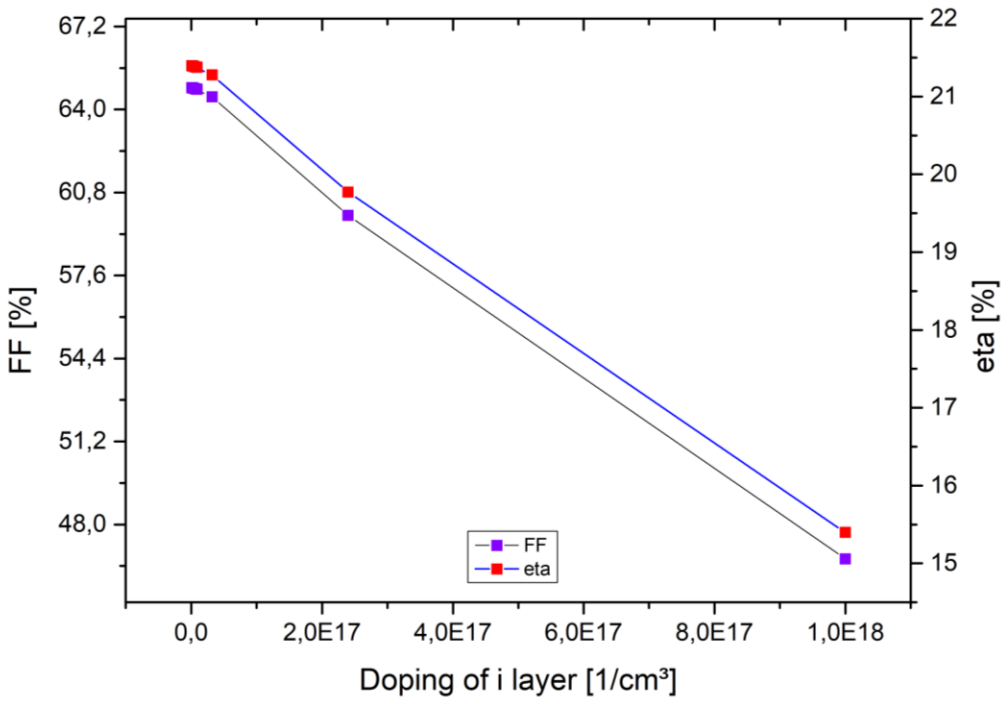

Fig III.9: The impact of the doping of i-layer on the device performances (FF,eta).

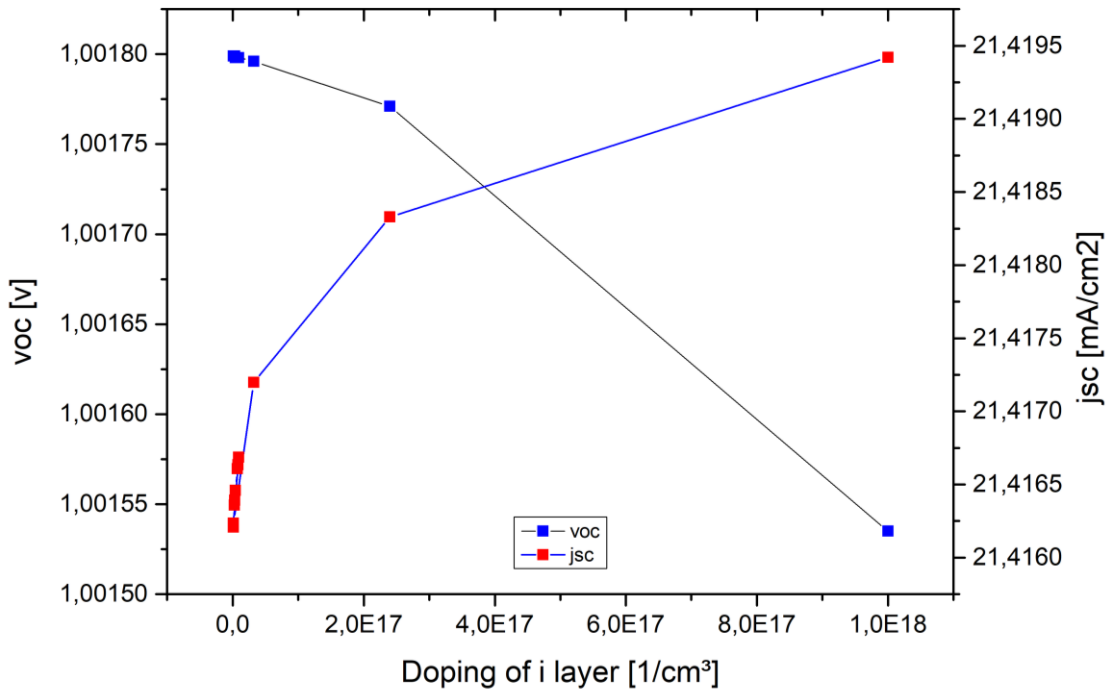

Fig III.10: *The impact of the doping of i-layer on the device performances (Voc,Jsc).*

III.5.2 The influence of ETL and HTL thickness on the device performance

Beyond light absorption by the perovskite layer, the n and p layers play a critical role in device performance. These layers efficiently transport generated charges (electrons and holes) to their respective electrodes. Additionally, they contribute to the device's high transparency, allowing more light to reach the active region. Furthermore, the thickness of these layers directly impacts the efficiency by influencing charge transport and recombination rates [1].

III.5.2.1 Effect of n-$FASnI_3$ thickness and doping concentration

We investigated the impact of n-$FASnI_3$ layer thickness (between 20 nm and 100 nm) on device performance, as shown in following Figures. While device performance generally improves with a thicker n-$FASnI_3$ layer, a balance is crucial. Interestingly, we also observed a positive correlation between doping level and efficiency, with the highest efficiency reaching 24.10 % at a doping level of 10^{20} cm^{-3} and fill factor (FF) of 73.08% at 10^{20}. Based on this analysis, we identified an optimal configuration for high device performance: a 300 nm thick p-layer,a 70 nm thick n-layer anda800nm thick n^+-$FASnI_3$layer.

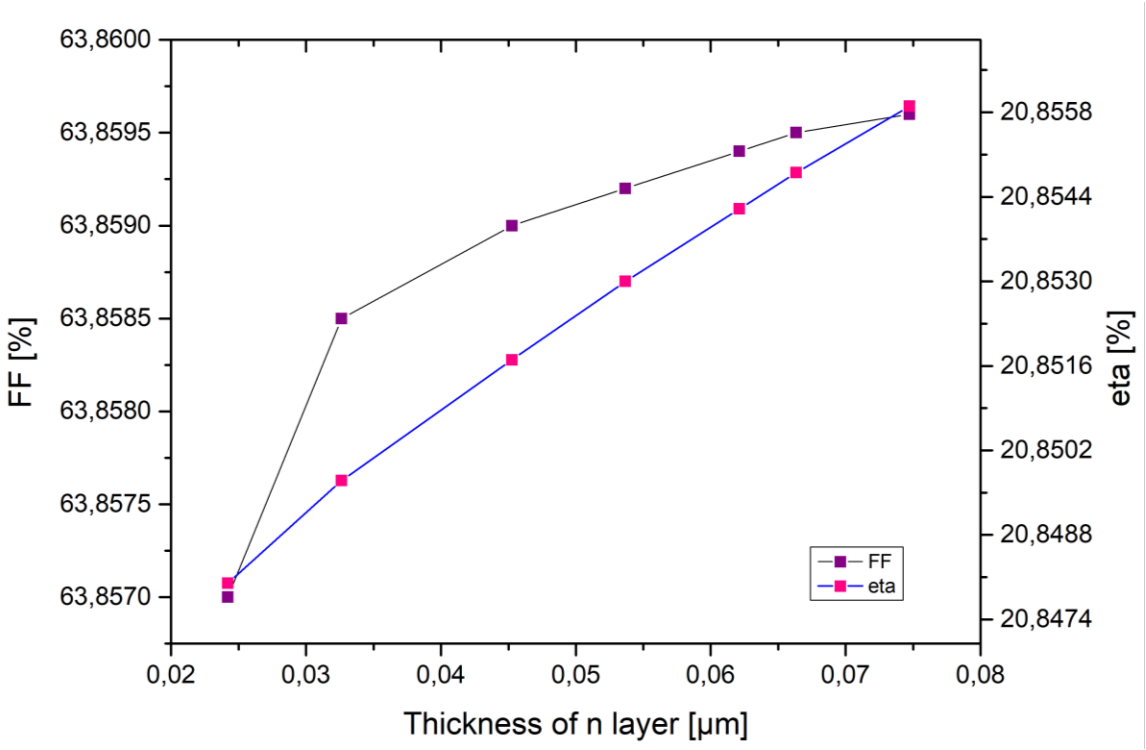

Fig III.11*: The impact of the thickness of n-layer on the device performances (FF,eta).*

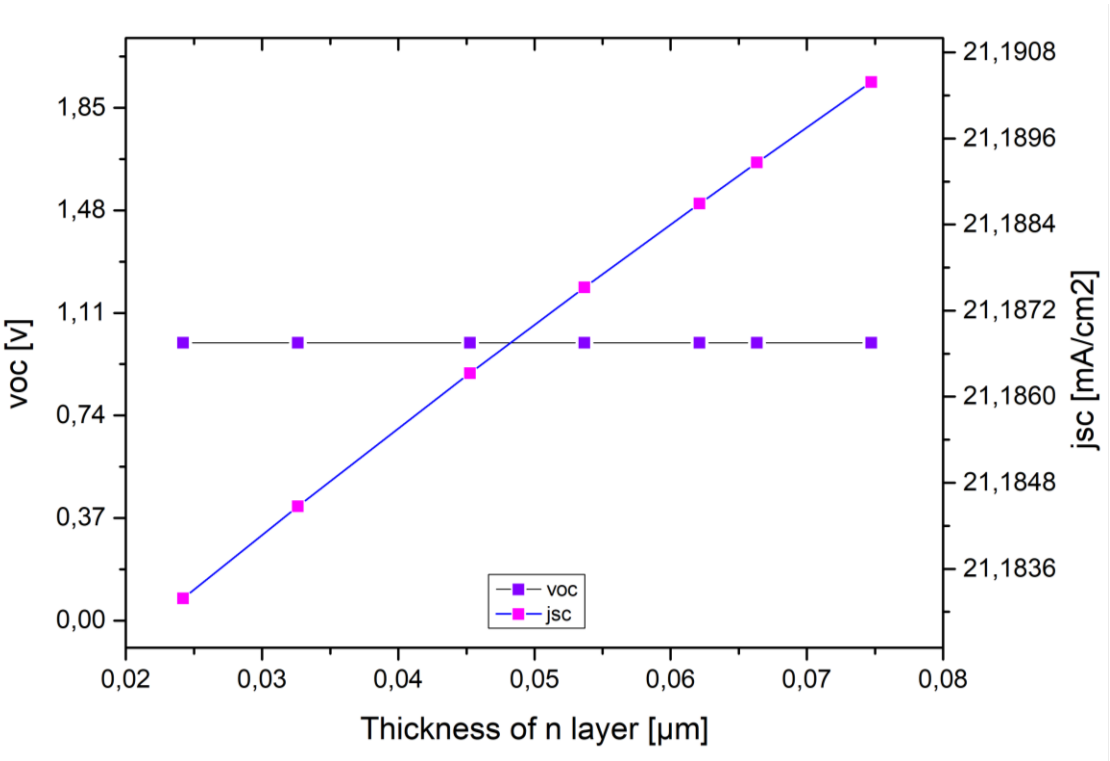

Fig III.12*: The impact of the thickness of n-layer on the device performances (Voc,Jsc).*

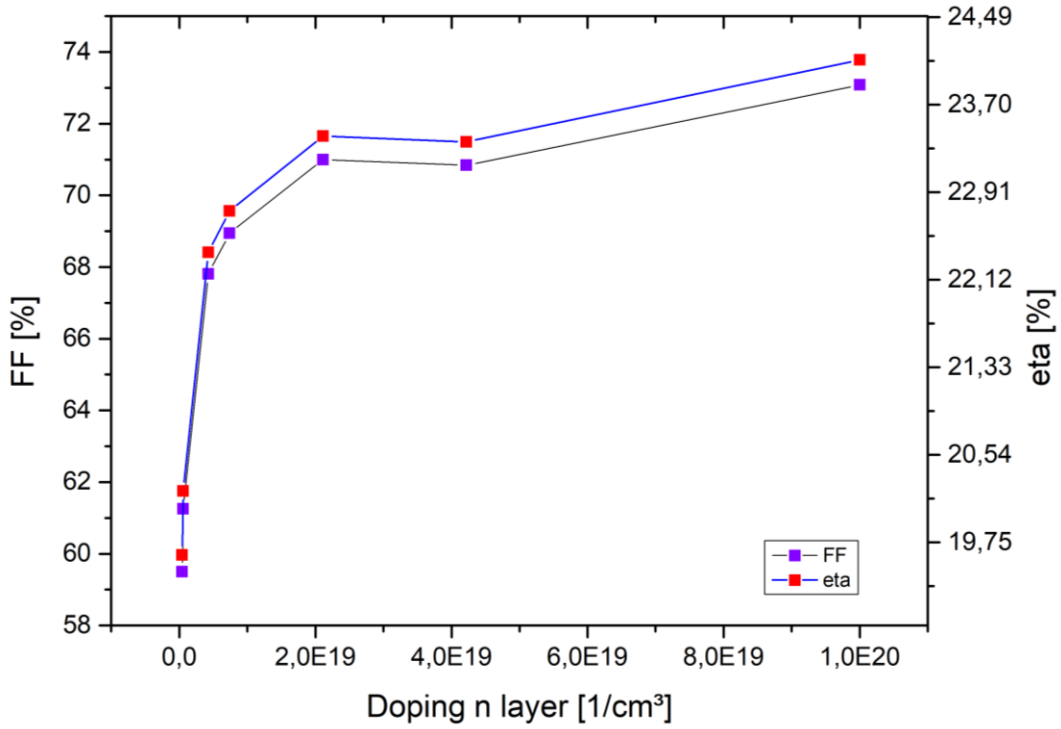

Fig III.13*: The impact of the doping of n-layer on the device performances (FF,Jeta).*

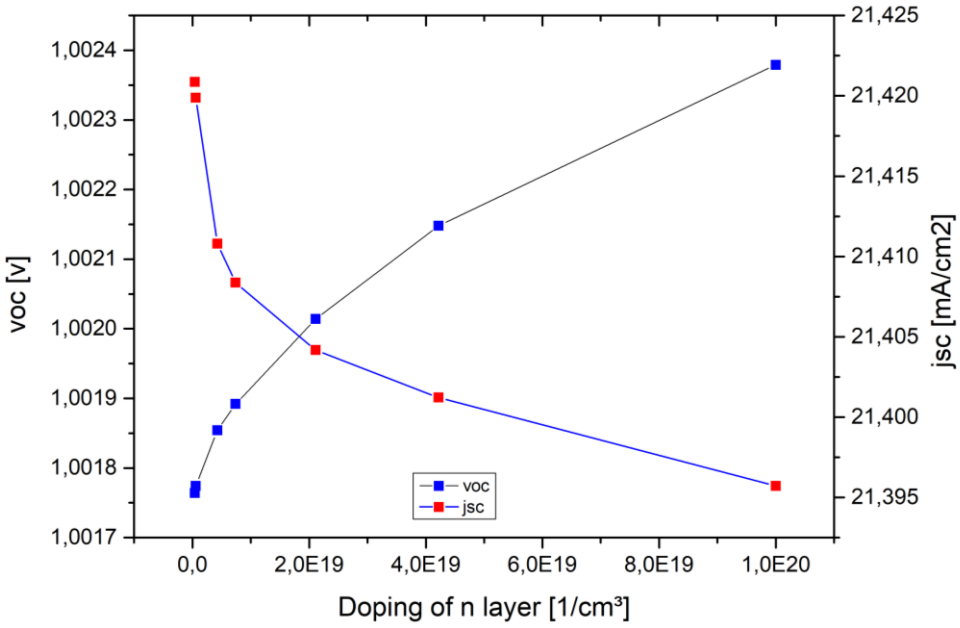

Fig III.14*: The impact of the doping of n-layer on the device performances (Voc,Jsc).*

III.5.2.2 Effect of p-$FAGeCl_3$ thickness and doping concentration

The device was simulated while increasing the thickness of p-layer between 100 nm and 1000 nm, The thicknesses of the i- $FASnI_3$, n-layer and n^+-$FASnI_3$ are chosen to be 800 nm and 70 nm,800 nm respectively. It is discovered that the performance of device would decline as p-layer thickness gets higher. To achieve high-efficiency, it is crucial to suitably limit the p layer thickness. Our experiments achieved a power conversion efficiency (PCE) of 20.90% for a p-layer thickness of 131 nm. In other words, thicker p-layers in our device led to lower efficiencies. Interestingly, we also found a positive correlation between doping level and device efficiency. When we increased the doping concentration, the efficiency climbed, reaching a peak of 23.84% at a doping level of 8.5×10^{21} $cm^{-3.}$ This suggests that optimizing the doping level is crucial for achieving high device efficiency.

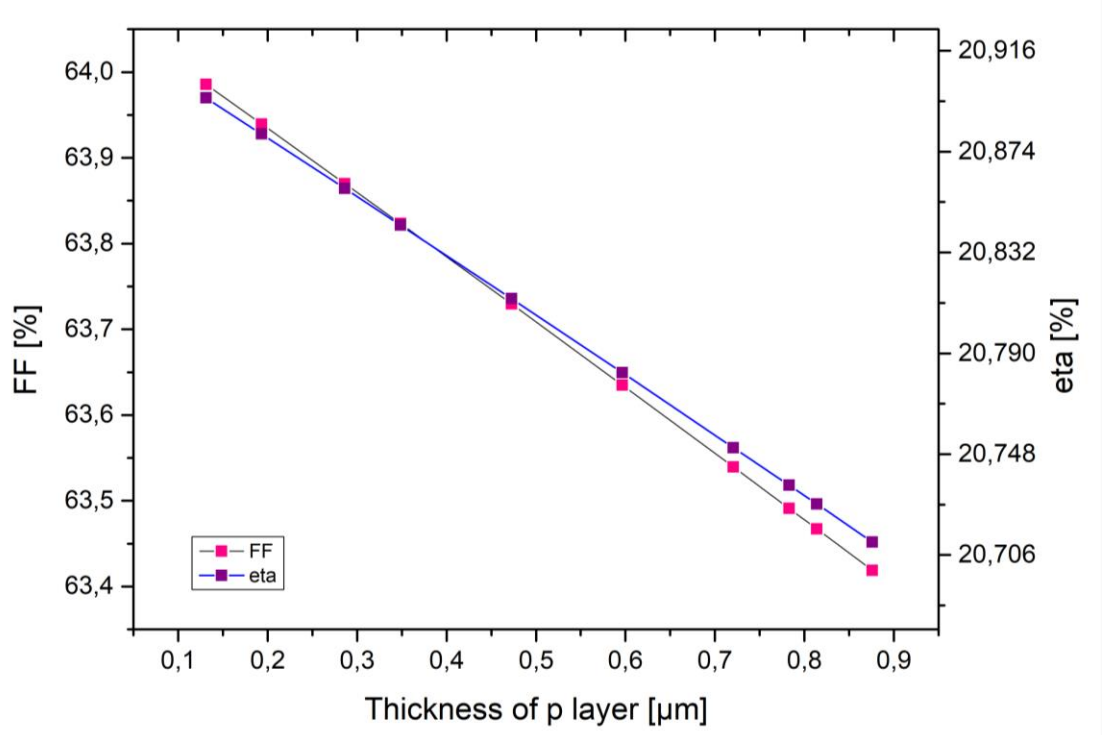

Fig III.15*: The impact of the thickness of p-layer on the device performances (FF,eta).*

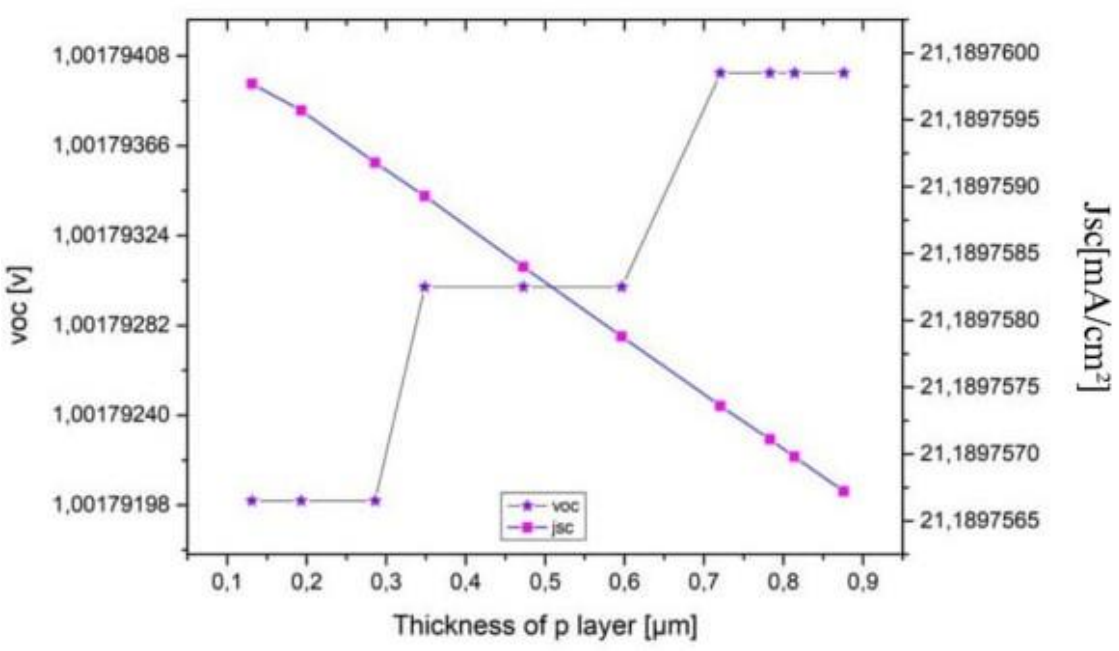

Fig III.16*: The impact of the thickness of p-layer on the device performances (Voc,Jsc).*

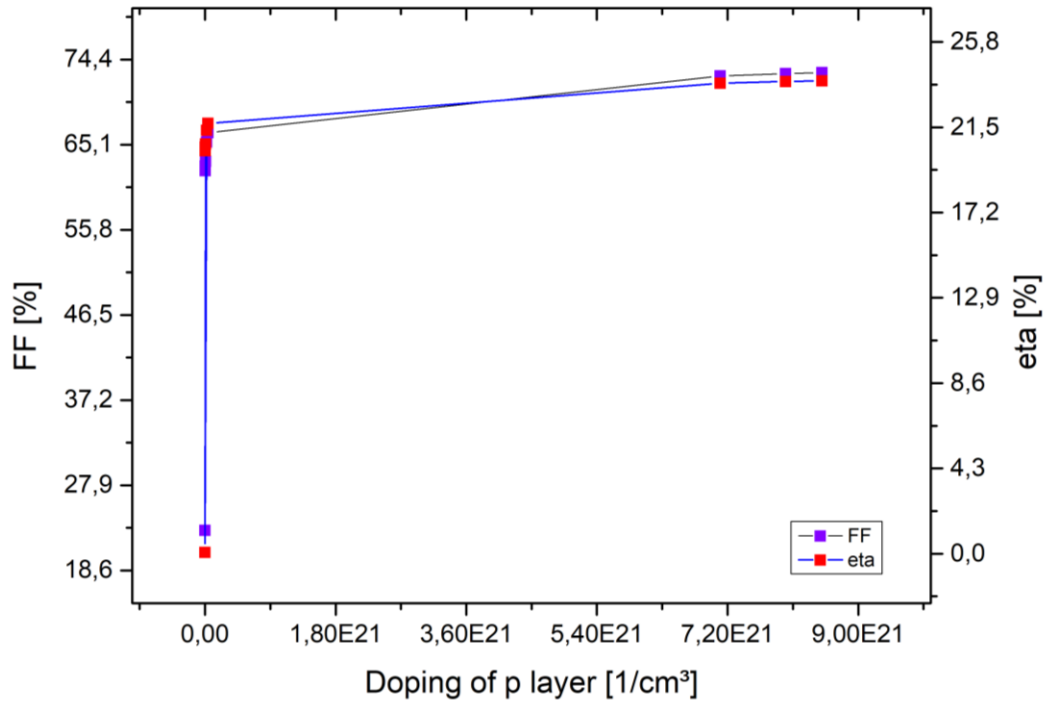

Fig III.17*: The impact of the doping of p-layer on the device performances (FF,eta).*

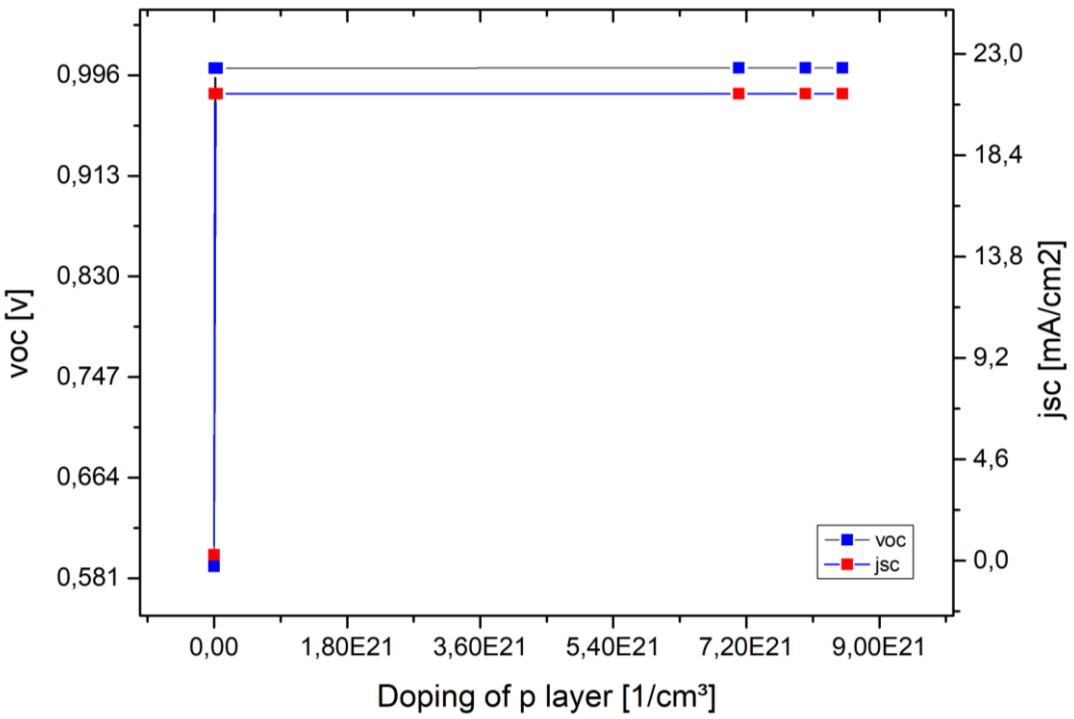

Fig III.18*: The impact of the doping of p-layer on the device performances (Voc,Jsc).*

III.5.3 Effect of n^+-$FASnI_3$ thickness and doping concentration on solar cell performance

This work introduces a heavily n-doped layer into the simulated device structure. However, heavy doping can alter the band gap of this layer, which (in this case) is set to be 1.4 eV to match the absorber layer. To achieve high carrier concentration without affecting the HOMO and LUMO energy levels, we should focus on manipulating carrier concentration rather than directly modifying the band gap.Several methods, such as band gap engineering, offer alternative approaches to high carrier concentration without significant changes to energy levels. Band gap engineering achieves this by adjusting the material composition to alter its electronic properties while minimizing HOMO-LUMO level shifts. This approach is particularly suitable for the studied ABX_3 perovskites due to their compositional flexibility and tunable band gaps [1].

To improve device performance (PCE) and minimize charge carrier loss at the FTO interface[1].This study investigates how thickness and carrier concentration within this layer strongly doped with electrons n^+-$FASnI_3$ affect overall performance. We varied the n^+-$FASnI_3$ thickness (100 nm - 1000 nm) and doping level ($10^{17}cm^{-3}$ - 10^{21} cm^{-3}) while keeping other layers fixed (n-$FASnI_3$: 70 nm, i-$FASnI_3$: 800 nm, p-$FAGeCl_3$: 300 nm). PCE significantly increases with n^+-$FASnI_3$ thickness, reaching a maximum of 20.92 % at 1000 nm. Doping level has a subtler effect. Increased doping leads to a rise in Voc, indicating reduced recombination of photo-generated charge carriers[1],and the highest efficiency (21.17%) achieved at a doping level of 6.7×10^{20} cm^{-3} and a fill factor ff of 64.82% at 10^{21} cm^{-3}.

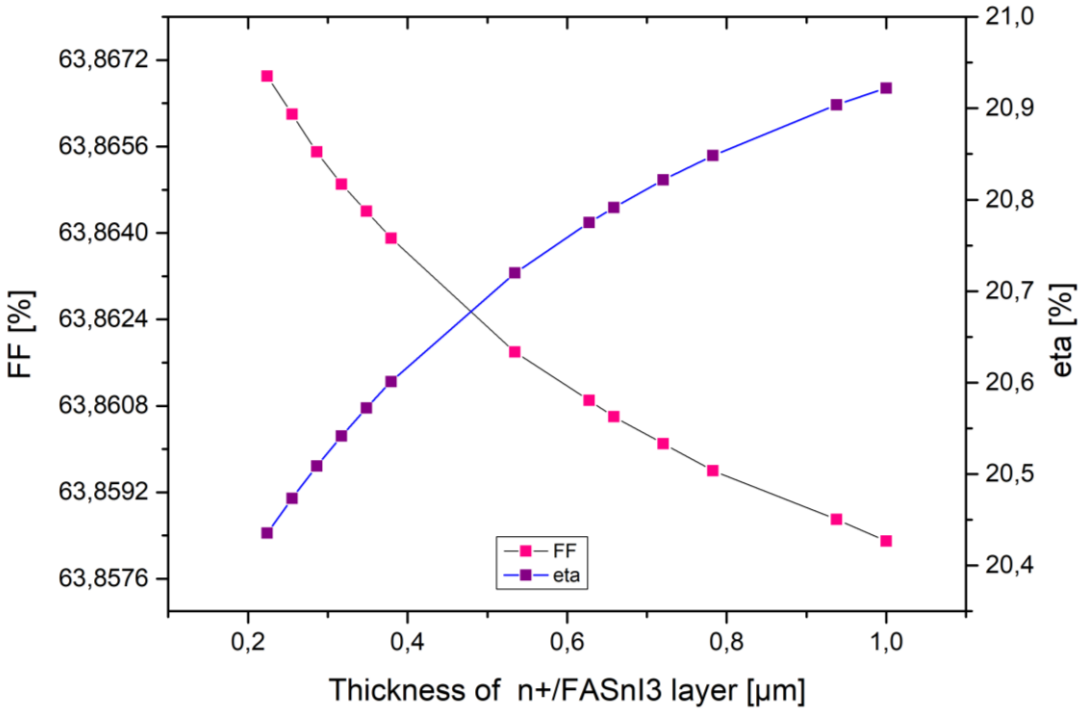

Fig III.19: *The impact of the thickness of n^+-$FASnI_3$ layer on the device performances (FF,eta).*

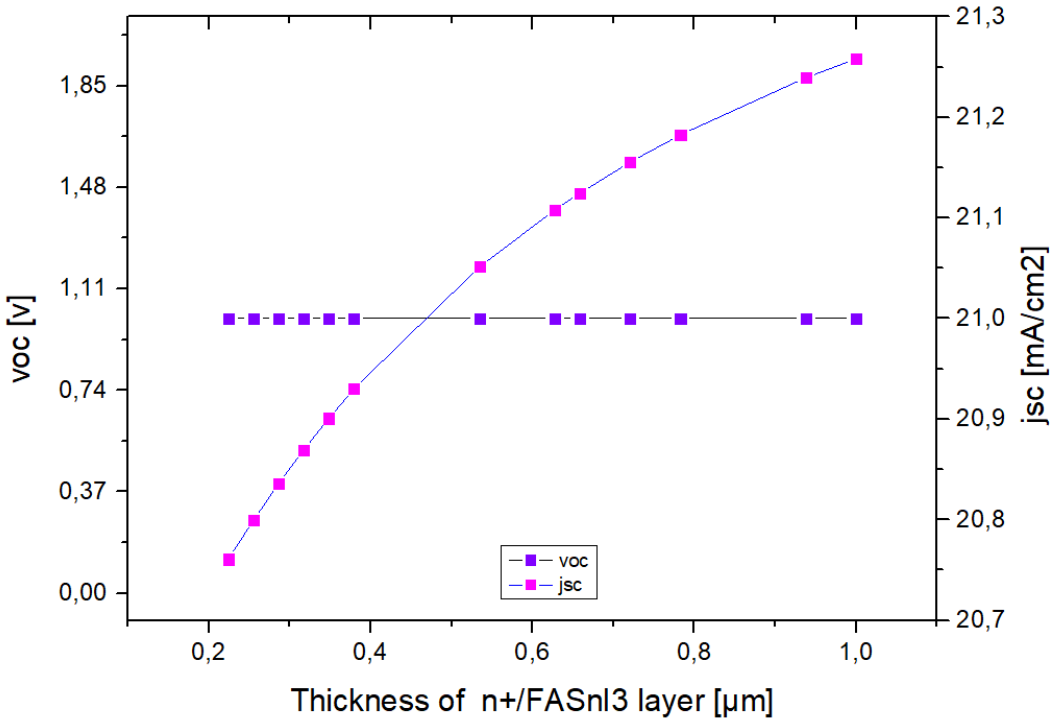

Fig III.20: *The impact of the thickness of n^+-$FASnI_3$layer on the device performances (Voc,Jsc).*

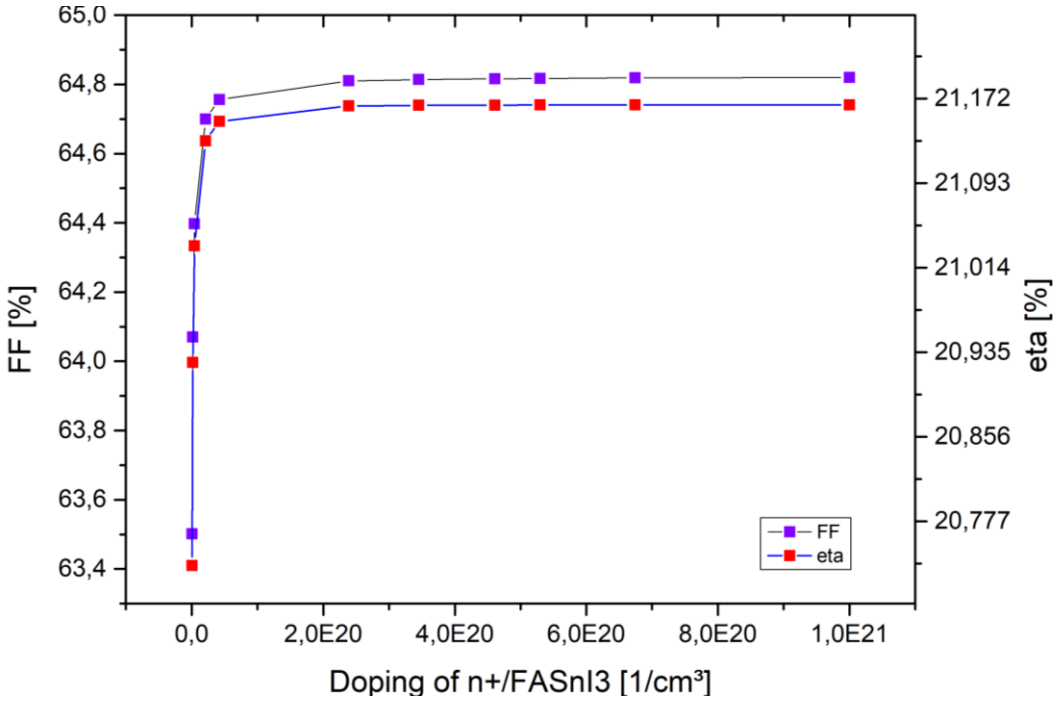

Fig III.21: *The impact of the doping of n^+-$FASnI_3$layer on the device performances (FF,eta).*

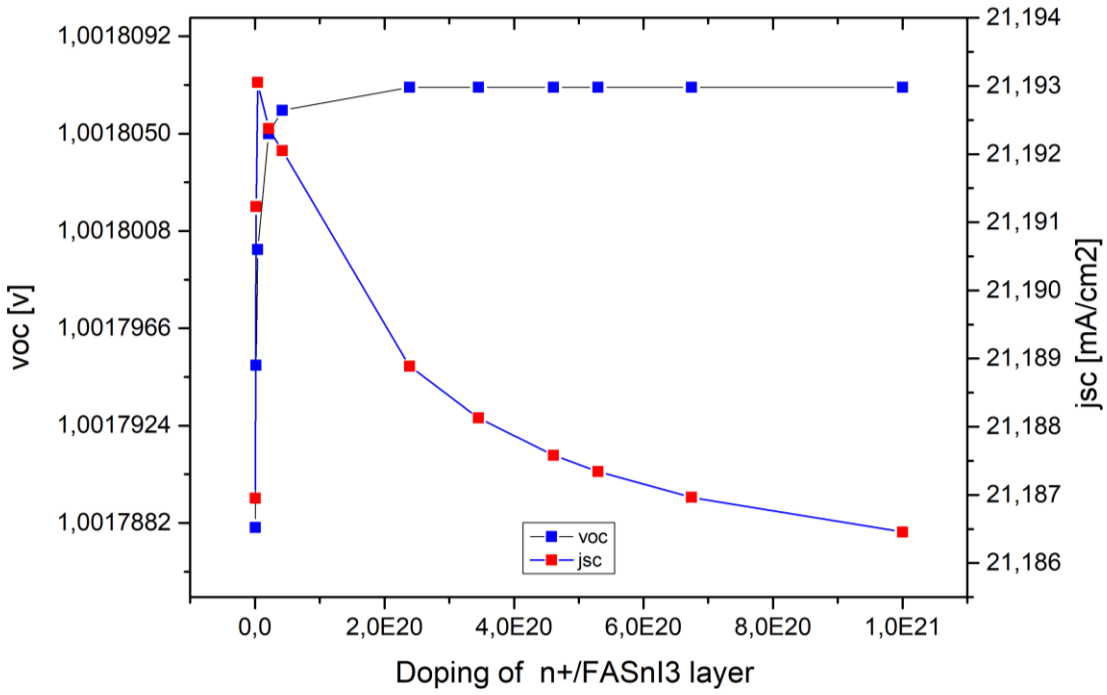

Fig III.22: *The impact of the doping of n^+-$FASnI_3$layer on the device performances (Voc,Jsc).*

III.6 CURRENT-VOLTAGE CURVE (I-V) AND QUANTUM EFFICIENCY (QE) OF THE SIMULATED DEVICE

Figure III.23 and **Figure III.24** show the positive impact of incorporating the n^+-$FASnI_3$ layer on both the current-voltage (J-V) characteristics and quantum efficiency (QE) of the device. The inclusion of this layer significantly enhances overall device performance. As the figure clearly demonstrates, the Jsc exhibits a notable improvement with the n^+-$FASnI_3$ layer. Additionally, the open-circuit voltage (Voc) increases due to the presence of n^+-$FASnI_3$.

This improvement in Voc can be attributed to the appropriate band alignment within the device structure. a higher band offset arising from the n^+-$FASnI_3$ layer leads to a greater built-in potential, ultimately boosting Voc. Figure illustrates the simulated device's QE across various wavelengths. The device exhibits remarkable absorption, reaching nearly 100% for certain wavelengths, which translates to a high rate of electron-hole pair generation. However, some limitations are evident. The losses observed in the QE figure for wavelengths below 400 nm are likely caused by reflection at the front face of the device. Conversely, the sharp decline in quantum efficiency for wavelengths exceeding 800 nm suggests increased recombination losses within the device[1].

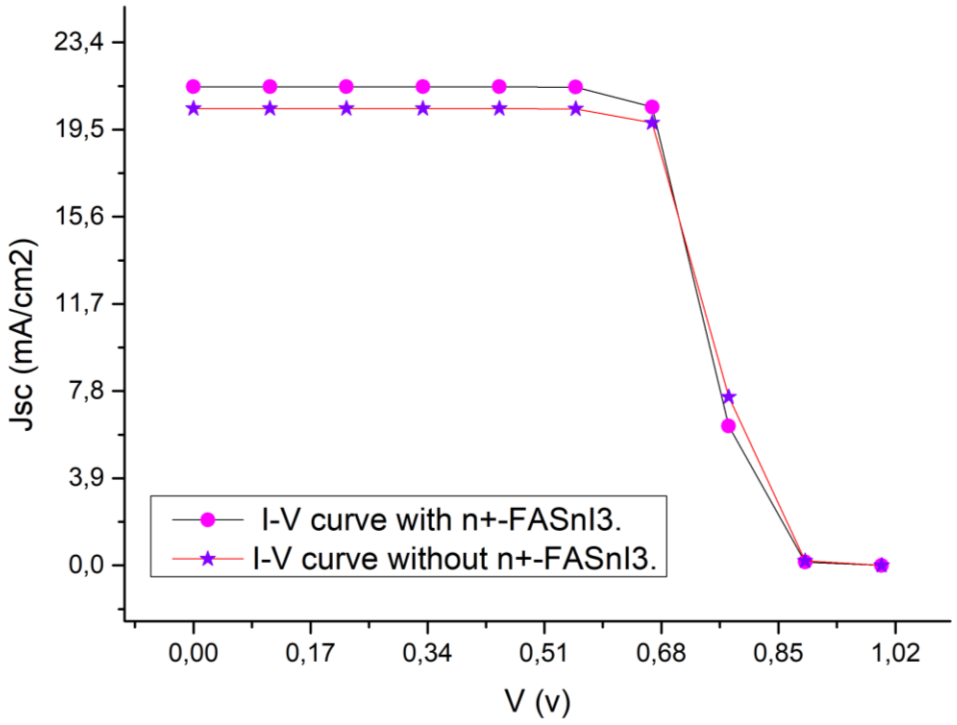

Fig III.23*: I-V curve of the device with and without n^+-$FASnI_3$.*

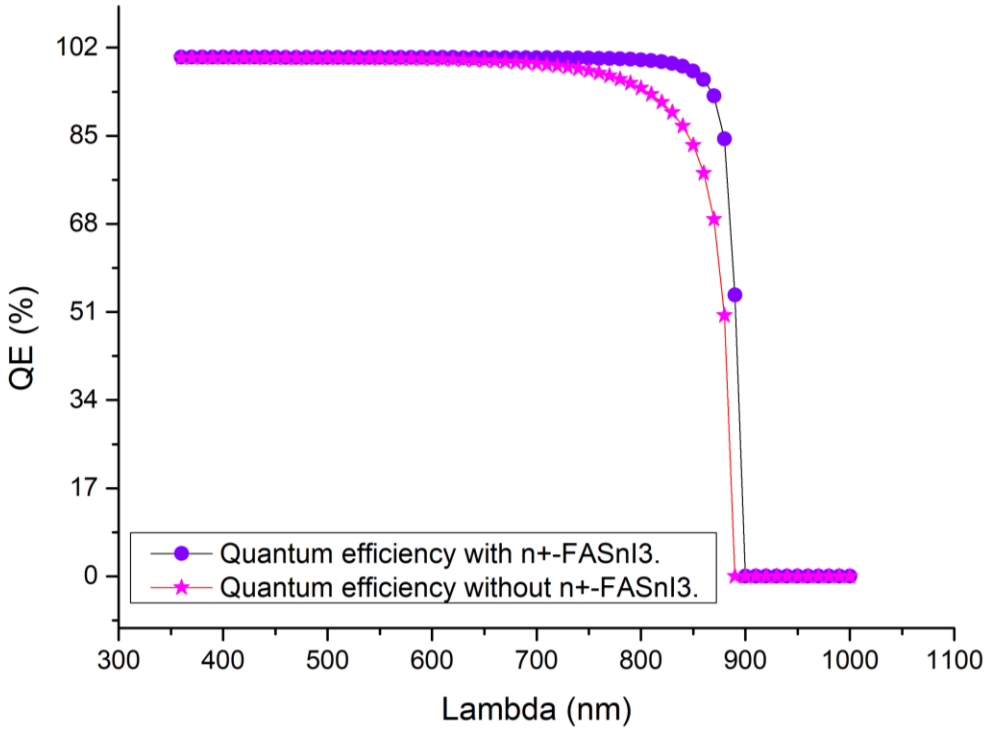

Fig III.24*: quantum efficiency of the device with and without n+-FASnI3.*

III.7 COMPARISONWITH PREVIOUS STUDIES

Table III.5: Performance of the proposed solar device with and without n^+-$FASnI_3$ compared with previous studies.

Solar cell architecture	Voc(V)	Jsc (mA/ cm2)	FF (%) P	PCE (%)
FTO/ n- FASnI3 i-FASnI3/p- FAGeCl3 Au.	**1.001805**	**20.44403526**	**64.8287**	**20.4187**
FTO/ n^+-FASnI3/n-FASnI3 i- FASnI3/p-FAGeCl3 /Au.	1.002379	21.39570570	73.0844	24.1042
$FASnI_3$ gradient (HTL-free structure) [3].				11.61
$FASnI_3$ gradient[3].				13.61

III.8 CONCLUSION

This simulation was employed to design and simulate a lead-free perovskite solar cell using SCAPS software with $FASnI_3$ as the light absorber. At 300 K, the efficiency is at its highest (PCE) of 20.41%, a fill factor (FF) of 64.83%, an open-circuit voltage (VOC) of 1.002 V, and a short-circuit current density (JSC) of 20.44 mA/cm².To improve performance, an n^+-$FASnI_3$ layer was introduced. The study revealed a significant impact of the intrinsic $FASnI_3$ (i-$FASnI_3$) layer thickness on PCE, as the thickness increased, the device performance improved. Optimization of the n-layer further enhanced the performance. However, increasing the p-layer thickness had the opposite effect.Ultimately, with the n^+-$FASnI_3$ layer incorporation, the optimized device achieved a maximum PCE of 24.10%, an FF of 73.08%, a VOC of 1.002 V, and a JSC of 21.40 mA/cm².

GENERAL CONCLUSION

In conclusion, this exploration of solar cells revealed the diverse landscape of this clean energy technology. We delved into the different generations, from first-generation crystalline silicon cells to third-generation.

our investigation into perovskite solar cells revealed a technology with the potential to revolutionize the photovoltaic landscape. Their unique crystal structure stands out as a key advantage, enabling superior light absorption across a broad spectrum of sunlight. This translates to the potential for significantly higher energy conversion efficiencies compared to traditional solar cell materials. Additionally, the inherent properties of perovskites make them incredibly versatile. They can be manufactured using cost-effective solution-processing techniques, opening doors for more affordable solar energy solutions. Furthermore, their ability to be deposited on flexible substrates allows for innovative and adaptable applications beyond traditional rigid solar panels.

Our research directly addressed these challenges by focusing on lead-free perovskite design. Utilizing SCAPS software, we designed and simulated a lead-free cell with an initial efficiency of 20.41%. To further enhance light absorption and overall performance, we incorporated an n+-FASnI3 layer and optimized the thickness and doping levels of various cell components. This optimization resulted in a significant efficiency increase to 24.10%.

These findings highlight the immense potential of perovskite solar cells and the ongoing efforts to overcome their limitations. By focusing on lead-free materials, optimizing light absorption properties, and improving cell stability, we can pave the way for a future where perovskite-based technologies play a pivotal role in meeting our growing energy demands in a sustainable manner.

REFRENCES AND BIBLIOGRAPHY

[1] Şen, Z. (2008). *Solar Energy Fundamentals and Modeling Techniques: Atmosphere, Environment, Climate Change and Renewable Energy*. London: Springer-Verlag.

[2] Bisquert, J. (2017). *The Physics of Solar Cells: Perovskites, Organics, and Photovoltaic Fundamentals*. Boca Raton, FL: CRC Press.

[3] Serdouk Mohammed Ridha, "*Etude par simulation numérique des propriétés*

électriques d'une cellule solaire en silicium amorphe hydrogéné (a-Si:H),"

MAGISTER, Université Mohamed Khider – Biskra, 2015.

[4] Tsen, K.-T. (Ed.). (2004). *Ultrafast Dynamical Processes in Semiconductors* (Vol. 92, Topics in Applied Physics). Springer Science & Business Media.

[5] Işık, T. (2015, January). *Solar Cells Review* [Bachelor's thesis, Işık University].

[6] Henry Mathieu et Hervé Fanet, *Physique des semi-conducteurs et des composants électroniques*, 6e édition, Dunod, Paris, 2009.

[7] Konate, R., Zouma, B., Mahamadi, S., & Barro, F. I. (2023). *Impacts of the base and emitter doping rate on the internal quantum efficiency*. In *2023* WOMEN IN PHYSICS: 7th IUPAP International Conference on Women in Physics .AIP Publishing..

[8] AA., & BB. (2015). Chapter X. In S. C. Bhatia (Ed.), *Advanced Renewable Energy Systems* (Location: New York). WPI Publishing.

[9] Warner, J. (2014, April). The Promise of Solar Energy in Our Daily Lives; *How Solar Cell Works*. *CHEMmatters*, p.

[10] Jackman, J. (2024, February 9).*The 9 Types of Solar Panels Explained***.** The EcoExperts. Accessed Feb 26.

[11] L. Pulfrey (1978). *Photovoltaic Power Generation*. Van Nostrand Reinhold Co., New York.

[12] J. Jean and B. P. (2015). "*Pathways for solar photovoltaics*," Energy Environ. *Sci.*, vol. 8, no. 4, pp. 1200-1219.

[13] Angermann, H., Conrad, E., Korte, L. et al. (2009) Passivation of textured substrates for a-Si:H/c-Si hetero-junction solar cells: *Effect of wet-chemical smoothing and intrinsic a-Si:H interlayer*. Materials Science and Engineering B.

[14] Wasilewski, Z. (2024, Feb 25). What is epitaxy? [Online]. *Molecular Beam Epitaxy*, University of Waterloo. Available: https://uwaterloo.ca/molecular-beam-epitaxy/about/what-epitaxy (Accessed: Feb 25, 2024).

[15] A. Shukla, M. Khare, and K. N. Shukla, "*Modeling and simulation of solar PV module on MATLAB/Simulink*," Int. J. Innov. Res. Sci. Eng. Technol., vol. 4, no. 1, pp. 172-176,Jan.2015.

[16] Nema, S., Nema, R. K., & Agnihotri, G. (2010). *Matlab/simulink based study of photovoltaic cells/modules/array and their experimental verification*. International journal of Energy and Environment.

[17] Petibon, S. (2009). *Nouvelles architectures distribuées de gestion et conversion de l'énergie pour les applications photovoltaïques* [New distributed architectures for energy management and conversion for photovoltaic applications]. PhD dissertation, Université Paul Sabatier-Toulouse III.

[18] J. W. Lee, D. H. Kim, H. S. Kim, S. W. Seo, S. M. Cho, and N. G. Park, "*Formamidinium and cesium hybridization for photo- and moisture-stable perovskite solar cell*," Adv. Energy Mater., 2015.

[19] Z. Li, M. Yang, J. S. Park, S. H. Wei, J. J. Berry, and K. Zhu, " *Stabilizing Perovskite Structures by Tuning Tolerance Factor: Formation of Formamidinium and Cesium Lead Iodide Solid-State Alloys*" Chem. Mater., 2016 .

[20] Huang, J., Xu, P., Liu, J., & You, X. Z. (2017). *Sequential Introduction of Cations Deriving Large-Grain CsxFA1−xPbI3 Thin Film for Planar Hybrid Solar Cells*: Insight into Phase-Segregation and Thermal-Healing Behavior. Small, 13(10), 1603225.

[21] Stenberg, J. (2017). *Perovskite solar cells* [Master's thesis, Umeå University]. Department of Physics, EN1731.

[22] Chia-Ming Lin and Cheng-Hao Kuei, *Investigation of the Effects of Various Organic Solvents on the PCBM Electron Transport Layer of Perovskite Solar Cells* Chih-Hung Tsai *,Published: 4 March 2020.

[23] Hussain, I., Tran, H. P., Jaksik, J., Moore, J., Islam, N., & Uddin, M. J. (2018). *Functional materials, device architecture, and flexibility of perovskite solar cell*. *IEEE Access*, 6, 74192-74221.

[24] Jiang, Q., Zhang, X., & You, J. (2018, août). *SnO2: A Wonderful Electron Transport Layer for Perovskite Solar Cells*. Small, 14(31), 1801154 (1-14). doi: 10.1002/smll.201801154.

[25] Kojima, A., Teshima, K., Shirai, Y., & Miyasaka, T. (2009, May). *Organometal halide perovskites as visible-light sensitizers for photovoltaic cells*. Journal of the American Chemical Society, 131(17), 6050-6051. doi: 10.1021/ja809598r.

[26] Jeng, J. Y., Chiang, Y. Y., Lee, M. H., & Wu, C. C. (2013, July*). CH3NH3PbI3 perovskite/fullerene planar-heterojunction hybrid solar cells*. Advanced Materials, 25(27), 3727-3732. doi: 10.1002/adma.201301327.

[27] Hu, Z., Xiang, H., Schoenauer Sebag, M., & al, e. (2018). *Compact layer free mixed-cation lead mixed-halide perovskite solar cells*. Chem. Commun, 54(21).

[28] Zheng, X., Hou, Y., Bao, C., & al, e. (2020, févr). *Managing grains and interfaces via ligand anchoring enables 22.3%-efficiency inverted perovskite solar cells*.

[29] Km Shivani Bhardwaj,Shambhavi Rai, Sadanand, Pooja Lohia, D.K.Dwivedi, *Investigating the performance of mixed cation mixed halide-based perovskite solar cells using various hole-transport materials bynumerical simulation*, Received: 27 April 2021 / Accepted: 18 September 2021.

[30] Hall, R. N. (1952). *Electron-Hole Recombination in Germanium*. *Phys. Rev.* 87(2), 387.

[31] Hawash, Z., Ono, L. K., & Qi, Y. (2018, Jan). *Recent Advances in Spiro-MeOTAD Hole Transport Material and Its Applications in Organic-Inorganic Halide Perovskite Solar Cells*. Advanced Materials Interfaces, 5(1), 1700623-22. doi: 10.1002/admi.201700623.

[32] Lin, L., Wang, J. T., Jones, T. W., & al, e. (2019*). Bulk recrystallization for efficient mixed-cation mixed-halide perovskite solar cells*. J. Mater. Chem.

[33] Song, S., Kang, G., Pyeon, L., Lim, C., Lee, G. -Y., Park, T., & Choi, J. (2017, déc). *Systematically Optimized Bilayered Electron Transport Layer for Highly Efficient Planar Perovskite Solar Cells*.

[34] LEMERCIER, T. (2020). *Développement de cellules solaires pérovskites semi-transparentes de type P-I-N dans la perspective d'une application tandem*. (U. S. BLANC, Ed.) Matériaux, Mécanique, Génie civil, Électrochimie, France.

[35] Ron Mertens,Oct 19,2023 ,*Perovskite Solar Agrivoltaics BIPV Indoor solar Perovskite solar production Perovskite-Info*.

[36] Wei, F., Zhao, Y., Deng, Z., Sun, S., & Li, D. (2020). *Strategies for Improving the Stability of Tin-Based Perovskite (ASnX3) Solar Cells*. Advanced Science, 7(3), 1903540.

[37] Wali, Q., Iqbal, Y., Pal, B., Lowe, A., & Jose, R. (2018, juin). *Tin oxide as an emerging electron transport medium in perovskite solar cells*.

[38] Spalla, M., Planes, E., Perrin, L., Matheron, M., Berson, S., &Flandin, L. (2019, oct). *Alternative Electron Transport Layer Based on Al-Doped ZnO and SnO2 for Perovskite Solar Cells Impact on Microstructure and Stability*. ACS Appl. Energy Mater., 2(10), 7183-7195. doi:10.1021/acsaem.9b01160.

[39] Z. Li, M. Yang, J. S. Park, S. H. Wei, J. J. Berry, and K. Zhu, "*Stabilizing Perovskite Structures by Tuning Tolerance Factor: Formation of Formamidinium and Cesium Lead Iodide Solid-State Alloys*," Chem. Mater., 2016.

[40] Weijun Ke , Constantinos C Stoumpos ,Mercouri G Kanatzidis , "*Unleaded*" Perovskites: Status Quo and Future Prospects of Tin-Based Perovskite Solar Cells, 2019 Nov;31(47):e1803230. doi: 10.1002/adma.201803230. Epub 2018 Oct 1.

[41] R. N. Hall, "*Electron-Hole Recombination in Germanium*," Phys. Rev., vol. 87, no. 2, pp. 387, Jul. 1952.

[42] W. Shockley and W. T. Read, Jr., "*Statistics of the Recombinations of Holes and Electrons*," Phys. Rev., vol. 87, no. 8, pp. 835, Sep. 1952.

[43] Sur les rayons β secondaires produits dans un gaz par des rayons X,Submitted by drupal on Sat, 04/28/2012 - 22:47,P. Auger, *«Sur les rayons β secondaires produits dans un gaz par des rayons X»* .

[44] R. Marschall, "*Adv. Funct. Mater*., vol. 24, no. None, pp. 2421–2440, 2014.

[45] Youssef El Arfaoui, Mohammed Khenfouch , Nabil Habiballah, December 2023,*Efficient all lead-free perovskite solar cell simulation of FASnI3/FAGeCl3 with 30% efficiency:* SCAPS-1D investigation.

[46] MA William, *Absorption study on the effect of mixed cation on tin and germanium-based perovskite solar cells*,2021.

[47] Tianhao Wu,Xiao Liu, Xinhui Luo, Hiroshi Segawa,Guoqing Tong,Yiqiang Zhang, Luis K. Ono, Yabing Qi and Liyuan Han , 08 April 2022. *Heterogeneous $FASnI_3$ Absorber with Enhanced Electric Field for High-Performance Lead-Free Perovskite Solar Cells.*

ملخص:

حازت الخلايا الشمسية البيروفسكايت غير العضوية اهتمامًا كبيرًا بسبب كفاءتها الملحوظة في تحويل ضوء الشمس إلى كهرباء. ومع ذلك، فقد أعاقت سمية الرصاص اعتمادها على نطاق واسع. تعالج هذه الدراسة هذا التحدي من خلال استكشاف $FASnI_3$كبديل خالٍ من الرصاص وصديق للبيئة. وباستخدام برنامج SCAPS ، قمنا بنمذجة هيكل الجهاز المتمثل في (FTO/n-$FASnI_3$ (ETL)/i-$FASnI_3$/p-$FAGeCl_3$ (HTL)/Au) حيث حققنا كفاءة أولية بنسبة 20.42%. ولتحسين الأداء بشكل أكبر، أضفنا طبقة مخدرة بقوةn^+- $FASnI_3$ ، مما زاد الكفاءة إلى 21.07%.و من خلال تغيير السمك ومستويات التخدير للطبقة i والطبقة n والطبقة p والطبقة n^+-$FASnI_3$ حققنا أعلى كفاءة بنسبة 24.10%. وتسلط هذه النتائج الضوء على $FASnI_3$كبديل واعد خالٍ من الرصاص قادر على تجاوز كفاءة الخلايا الشمسية البيروفسكايتية غير العضوية التقليدية القائمة على الرصاص، مما يمهد الطريق لمستقبل أكثر استدامة وصديقة للبيئة في مجال الطاقة الشمسية.

الكلمات المفتاحية: خلايا البيروفسكايت الشمسية، $FASnI_3$، برنامج SCAPS.

Abstract

Inorganic perovskite solar cells have attracted significant attention for their remarkable efficiency in converting sunlight into electricity. yet, their widespread adoption has been hindered by the toxicity of lead. This study addresses this challenge by exploring $FASnI_3$ as a lead-free and environmentally friendly alternative. Using SCAPS software, we modeled the device structure of (FTO/n-$FASnI_3$(ETL)/i-$FASnI_3$ /p-$FAGeCl_3$(HTL)/Au) and achieved an initial efficiency of 20.42%. To further improve performance, we added a strongly n-doped layer n^+ -$FASnI_3$, which increased efficiency to 21.07%. And by varying the thickness and doping levels of (i-layer, n-layer, p-layer, and
($n^+$$FASnI_3$), we achieved the highest simulated efficiency of 24.10%. These results highlight $FASnI_3$ as a promising lead-free alternative capable of exceeding the efficiency of conventional lead-based inorganic perovskite solar cells, paving the way for a more sustainable and environmentally friendly future in solar energy.

Keywords: perovskite solar cells, FASnI 3 ,SCAPS software.

Resumé:

Les cellules solaires pérovskites inorganiques ont attiré l'attention pour leur remarquable efficacité à convertir la lumière du soleil en électricité. Pourtant, leur adoption à grande échelle a été entravée par la toxicité du plomb. Cette étude relève ce défi en explorant $FASnI_3$ comme une alternative sans plomb et respectueuse de l'environnement. À l'aide du logiciel SCAPS, nous avons modélisé la structure du dispositif (FTO/n-$FASnI_3$ (ETL)/i-$FASnI_3$ /p- $FAGeCl_3$ (HTL)/Au) qui a obtenu un rendement initial de 20,42%. Pour améliorer encore les performances, nous avons ajouté une couche fortement dopée n + - FASnI 3 , ce qui a permis d'augmenter l'efficacité à 21,07 %. Et en variant l'épaisseur et les niveaux de dopage de les couches (i-layer, n-layer, p-layer, and n^+ -$FASnI_3$), nous avons obtenu le rendement simulé le plus élevé, soit 24,10 %. Ces résultats montrent que $FASnI_3$ est une alternative prometteuse sans plomb capable de dépasser l'efficacité des cellules solaires pérovskites inorganiques conventionnelles à base de plomb, ouvrant ainsi la voie à un avenir plus durable et plus respectueux de l'environnement dans le domaine de l'énergie solaire.

Mots-clés: cellules solaires pérovskites, FASnI3, logiciel SCAPS.